





## Article

# Spatial and Temporal Patterns of Land Subsidence and Sinkhole Occurrence in the Konya Endorheic Basin, Turkey

Osman Orhan <sup>1</sup>, Mahmud Haghshenas Haghghi <sup>2</sup>, Vahdettin Demir <sup>3</sup>, Ergin Gökkaya <sup>4</sup>, Francisco Gutiérrez <sup>5</sup>  
and Djamil Al-Halbouni <sup>6,\*</sup>

<sup>1</sup> Department of Geomatics, Engineering Faculty, Mersin University, 33343 Mersin, Turkey; osmanorhan@mersin.edu.tr

<sup>2</sup> Institute of Photogrammetry and GeoInformation, Leibniz University Hannover, Nienburger Str. 1, 30167 Hannover, Germany; mahmud@ipi.uni-hannover.de

<sup>3</sup> Department of Civil Engineering, Faculty of Engineering and Natural Sciences, KTO Karatay University, 42020 Konya, Turkey; vahdettin.demir@karatay.edu.tr

<sup>4</sup> Department of Geography, Faculty of Sciences and Letters, Niğde Ömer Halisdemir University, 51240 Niğde, Turkey; erginngokkaya@gmail.com

<sup>5</sup> Department of Earth Sciences, Faculty of Sciences, University of Zaragoza, 50009 Zaragoza, Spain; fgutier@unizar.es

<sup>6</sup> Institute for Earth System Science and Remote Sensing, Faculty of Physics and Earth System Sciences, Leipzig University, 04103 Leipzig, Germany

\* Correspondence: dhalbouni@uni-leipzig.de

**Abstract:** The endorheic Konya Basin is a vast aggradational plain in Central Anatolia, Türkiye. It occupies a significant portion of Konya Province, covering approximately 50,000 km<sup>2</sup>. The basin is subjected to intense groundwater withdrawal and extensive agricultural activities with excessive irrigation. These activities have led to human-induced hazards, such as sinkholes and regional land subsidence. Although sinkhole occurrence mainly occurs in the Karapınar area, land subsidence is primarily observed in the central sector of Konya city, with 2 million inhabitants, as well as in various parts of the basin. This study focuses on determining the extent and rate of land subsidence throughout the basin, understanding sinkhole formation, and unraveling their relationship with anthropogenic activities. For this purpose, Interferometric Synthetic Aperture Radar (InSAR) analysis of Sentinel-1 data from 2014 to 2022 was conducted to identify and assess land subsidence. We also used the land cover data and groundwater-level information to better understand the spatial and temporal patterns of land subsidence and sinkhole occurrence. Additionally, the land cover data were used to resolve spatial–temporal variations in the cultivated area and urbanization, which are the main factors governing groundwater exploitation in the region. Our study identified widespread subsidence zones with rates as high as 90 mm/y. Groundwater overexploitation to sustain extensive agricultural operations is the main cause of the high rate of land subsidence. Additionally, it was discovered that the number of sinkholes has substantially increased due to anthropogenic influences, currently amounting to as many as 660.

**Keywords:** Konya Closed Basin; sinkhole; land subsidence; Sentinel-1; InSAR



**Citation:** Orhan, O.; Haghshenas Haghghi, M.; Demir, V.; Gökkaya, E.; Gutiérrez, F.; Al-Halbouni, D. Spatial and Temporal Patterns of Land Subsidence and Sinkhole Occurrence in the Konya Endorheic Basin, Turkey. *Geosciences* **2024**, *14*, 5. <https://doi.org/10.3390/geosciences14010005>

Academic Editors: Mimmo Palano and Jesus Martinez-Frias

Received: 2 November 2023

Revised: 18 December 2023

Accepted: 20 December 2023

Published: 22 December 2023



**Copyright:** © 2023 by the authors. Licensee MDPI, Basel, Switzerland. This article is an open access article distributed under the terms and conditions of the Creative Commons Attribution (CC BY) license (<https://creativecommons.org/licenses/by/4.0/>).

## 1. Introduction

Karst landscapes are characterized by the predominance of subsurface drainage and distinctive landforms associated with soluble rocks, such as carbonates and evaporites [1]. Karst landforms cover a wide range of sizes, from millimeters to hundreds of kilometers (e.g., karren, sinkholes, caves, poljes, monoclinical scarps atop dissolution fronts), and are primarily created by solutional denudation in the surface and subsurface [2]. Essentially, subsurface dissolution by undersaturated groundwater with respect to the constituent minerals of the surrounding rocks results in the development of permeability and underground drainage systems through which solute load is transported. Subsidence related

to subsurface dissolution is one of the most important morphogenetic processes in karst terrains. Solutional mass removal at depth may lead to the gravitational deformation (collapse, sagging) and/or internal erosion (subrosion) of the overlying undermined material. These subsidence phenomena can display a wide spectrum of spatial and temporal patterns, ranging from small catastrophic sinkholes to regional subsidence structure-related long-term interstratal dissolution of evaporites [2].

About 40% of the area in Türkiye is underlain by rocks suitable for karstification (ca. 300,000 km<sup>2</sup>), and six major karst regions have been identified in the country [3]. The Central Anatolian Karst Region (CAK) is a semi-arid continental area surrounded by the Taurus Mountains Karst in the south, the Thrace and Black Sea Mountains Karst in the north, and the Eastern and Western Anatolian Karst [3]. Tectonically, the CAK lies at the center of the Anatolian microplate within the Arabia–Eurasia convergence realm, characterized by substantial neotectonic deformation [4]. The plateau is bounded by NE–SW and NW–SE (Sultanhanı Fault as part of the Eskişehir Fault zone, Tuz Gölü Fault) trending faults, and its tectonic evolution as an endorheic basin is related to an extensional regime that took place mainly during Miocene–Early Pliocene times [5], but active normal faults are also present today.

At the southern sector of the CAK, the Konya Basin is a high-elevation and low-relief region [6] lying between 1050 and 1350 m a.s.l. [3]. It contains the dried-out pluvial Konya paleolake and the residual Salt Lake (Tuz Gölü in Turkish) (Figure 1) [7–9]. The Akşehir Lake closed basin to the north also forms part of the CAK.

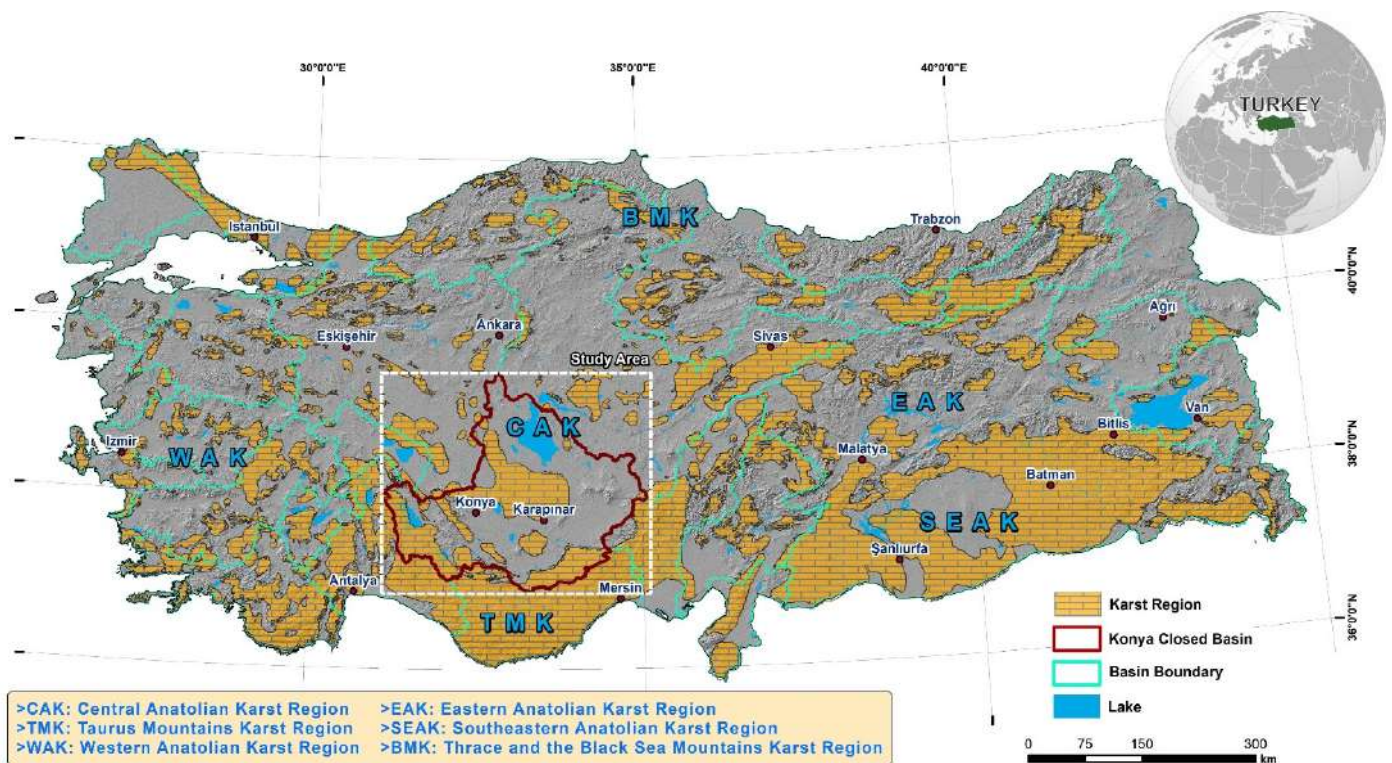


Figure 1. Distribution of the main karst regions in Türkiye (modified from [9]).

In a number of regions in the world, hypersaline lakes show extremely high rates of water-level drop, such as Urmia Lake in NW Iran [10], the Dead Sea [11] in the Middle East, and Salt Lake in central Türkiye [7,12]. Anthropogenic salt production and the use of water resources (Dead Sea, Salt Lake) have been identified as the main reasons for the decrease in the water levels (e.g., [13–16]), whereas at Urmia Lake, recovery programs are currently being implemented [17].

Worldwide, sinkholes are among the most significant geological hazards in karst areas, leading to negative consequences in terms of economic losses and loss of human

life [18–20]. Some of the most destructive sinkholes have formed in Wink, TX, USA [21]; southeastern Minnesota, USA [22]; Nash Draw, southeastern New Mexico, USA [23]; Tournaisis, southern Belgium [24]; Apulia, southern Italy [25]; Naples, southern Italy [26]; Ebro River valley, Spain [27]; the shores of the Dead Sea [28,29]; Hamedan, Iran [30]; Sivas, Turkey [31]; Konya, Turkey [14]; and Karapınar, Turkey [32,33]. Gutiérrez (2016) provided a compilation of some of the most damaging sinkhole events in carbonate and evaporite karst areas [34].

Paleoclimate reconstructions indicate that cold and wet environmental conditions in the Eastern Mediterranean during the Last Glacial Maximum led to lake-level highstands between 20 and 22 ka [35]. The transition between wet and dry periods was recorded by the deposition of evaporites in some lakes, as determined by borehole data [36]. Recent dating situates the highstand of Konya Lake at around 28~21.7 ka, lasting sufficient time for the development of wave-cut landforms in the Jurassic and Pliocene carbonates exposed at the northern shore of the Konya paleolake [6].

The Karapınar Hotamış plain is a desiccated sub-basin of the Konya paleolake [37]. Research has focused on this area since the 2000s because of the increasing occurrence of cover collapse sinkholes [38–41]. Sinkholes in Turkish are commonly designated as *obruks*, mainly referring to as collapse sinkholes, which reach hectometer-scale diameters in the limestone plateau within the Konya Basin of central Türkiye [42]. These *obruks*, which often form catastrophically and with sizes ranging between a few meters and tens of meters in diameter (Figure 2), can cause detrimental effects on agriculture, infrastructure, and human safety, as documented in many places worldwide [15,43–48]. Sinkholes that have occurred since 1970 are considered new depressions potentially induced by human activity, whereas other depressions, especially the numerous degraded bedrock collapse sinkholes, may have formed a long time ago in Quaternary and Neogene times and under different environmental conditions [49]. The formation process has been attributed to the collapse of cavities created in Neogene limestones by rising undersaturated groundwater in a hypogenic karst system. Older, buried sinkholes (i.e., paleosinkholes) are also observable in exposures of Permian to Triassic marbles and Jurassic to Cretaceous limestones [3] at elevations of up to 550 m above the basin floor. Their potential role in the desiccation of the Konya paleolake is still under debate [3]. The aggressiveness of the rising water can be renewed/enhanced by the incorporation of deep-sourced CO<sub>2</sub> of volcanic origin. Most probably, cavity-roof instability has been induced in recent times by the escalating groundwater-level drop caused by aquifer overexploitation [49,50]. Recently, various types of sinkhole susceptibility maps have been developed to help local authorities identify the most hazardous areas and mitigate the potential detrimental effects of new sinkholes [15].

However, sinkholes have also occurred recently in other areas around the paleolake, such as in basin floor and in alluvial deposits around the dried-out lake in Seyithacılar village in the Hotamış and Çumra area. Remote sensing studies analyzing recent subsidence patterns in the whole Konya Basin are lacking. Here, we focus on the Interferometric Synthetic Aperture Radar (InSAR) analysis of the distribution of recent high-rate subsidence areas and the role played by anthropogenic factors. We aim to answer the following main questions: Where does the subsidence occur? What are the spatial patterns of sinkhole formation? Which region is the most active (i.e., most hazardous one)? Is there a relation between the highstand shorelines of the Konya paleolake and the distribution of subsidence phenomena? What is the relation between the groundwater flow directions and subsidence processes? Can we decipher specific hydrogeologic conditions for subsidence development?



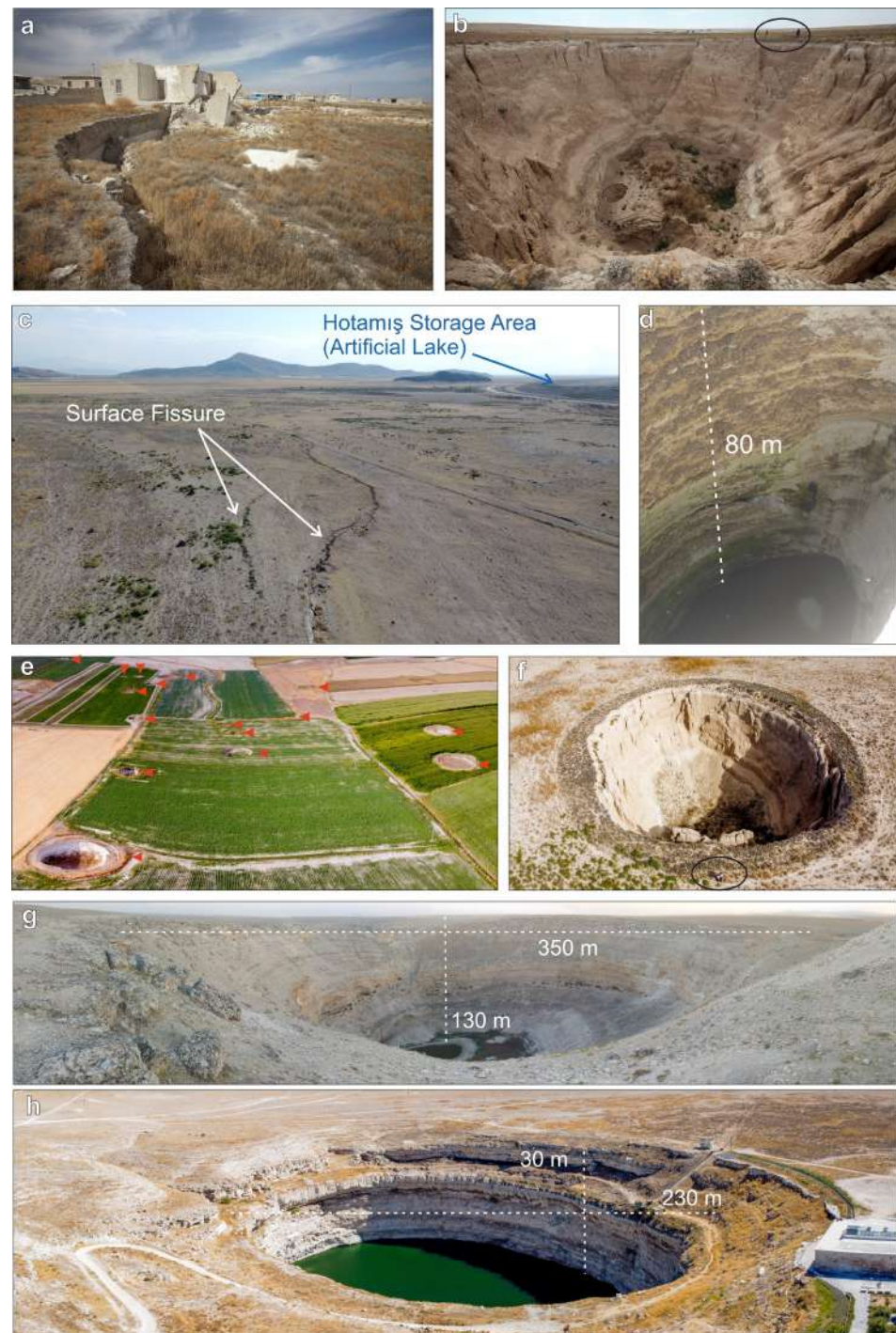


**Figure 2.** Examples of recent cover collapse sinkholes (obruks) and old bedrock collapse sinkholes in the Konya Basin. (a) Sinkhole that destroyed a building in Seyit Hacı village. (b) Kolca Yayla Obruk, with nested collapse holes in the floor. (c) Surface fissures–scarps located near the Hotamış storage area. (d) Akviran sinkhole 80 m deep and 25 m across. (e) Cover collapse sinkhole cluster with a distinct linear distribution north of Karapınar. These sinkholes formed after 2011. The red triangles indicate the location of the sinkholes. (f) Sekizli cover collapse sinkhole. Note the arcuate cracks at the margin of the sinkhole, which are the initial stage of mass movements. (g) The old Çıralı sinkhole, which hosts many artificial cave houses (h) The old Kızören bedrock collapse sinkhole. The distinctive ledge on the steep margin of the sinkhole is associated with calcareous tufas deposited underwater during a high water table level. The sinkhole, which hosts a permanent lake, is about 100 m deep. The circles indicate people for scale.

## 2. Study Area and Hydrogeology

The endorheic Konya Basin, covering over 50,000 km<sup>2</sup>, is located in the southern sector of the Central Anatolian Plateau, lying at approximately 1000 m a.s.l. (Figure 1). The Konya Basin includes the NW–SE-trending Beyşehir and Suğla sub-basins in the western sector of the basin, north of the Taurus Mountains; the V-shaped Konya–Karapınar sub-basin in the south; and the Tuz Lake sub-basin in the north (Figure 3).

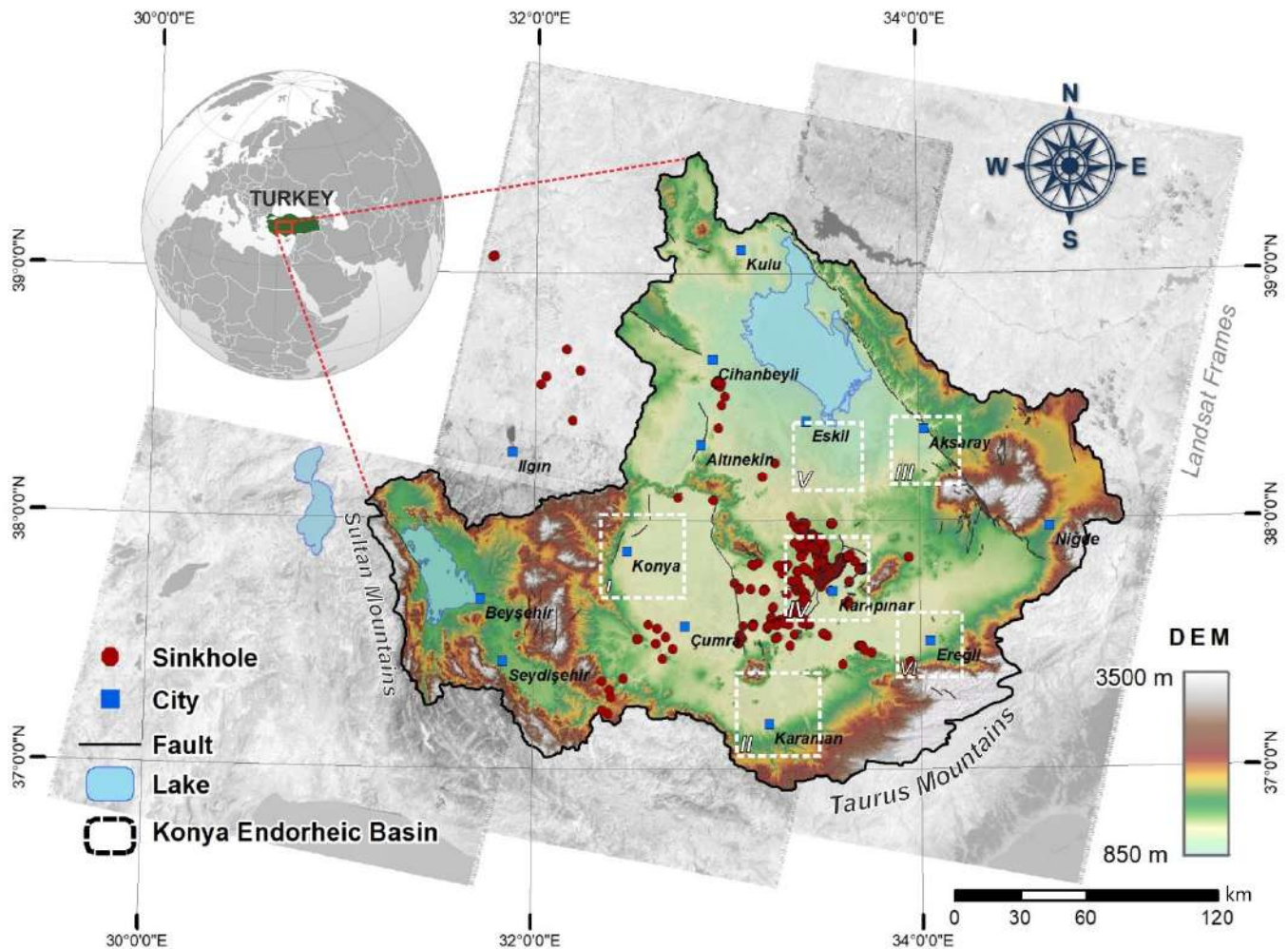


**Figure 3.** Location of the study area on a digital elevation model. Red circles mark the location of sinkholes. White frames I, II, and III mark the location of Figure 6a–c, respectively. White frames IV, V, and VI mark the location of Figure 7a–c, respectively.

The endorheic Konya Basin is located between 36°51' N and 39°29' N latitude and between 31°36' E and 34°52' E longitude. Geographically, the Konya Basin is surrounded by high mountain ranges such as the Sultan Mountains to the west and the Taurus Mountains to the south [15]. These ranges define the divides of this hydrologically closed basin, limiting surface and underground water inflow and outflow. In addition, outcrops of recent volcanic rocks such as the Karacadağ Mountain, the Erenler Mountain, and the Takkeleli Mountain form topographic highs within the basin. The endorheic Konya Basin has a complex hydrogeology with significant underground water resources. The water of the Büyük Menderes River and the groundwater recharged in the Taurus Mountains flow underground, forming significant karst water resources. Groundwater levels decrease progressively due to the excessive use of water resources and the arid climatic conditions of the basin [14]. This situation not only threatens the sustainability of water resources but also induces the formation of sinkholes that cause social and economic damage [51]. Our



cartographic sinkhole inventory was obtained from the State Hydraulic Works (DSİ). This inventory was updated with field studies carried out in 2023 and orthoimages from 2021 and 2022. The inventory includes a total of 660 sinkholes located within the basin. Additionally, chemical fertilizers and pesticides used in agricultural areas cause groundwater-quality problems in the region.

The basin has a continental climate characterized by hot summers and cold winters with considerable spatial variability. Whereas the climate demonstrates Mediterranean features in Beyşehir and its surroundings in the southwest, a semi-arid climate prevails in most of the endorheic basin. The driest zone corresponds to the Karapınar area, which is the region with the least rainfall in Türkiye (270 mm/y). The mean annual precipitation varies between 250 mm and 400 mm [52–54], with considerable potential for droughts. Despite the shortage of precipitation in the basin and the limited aquifer recharge, extensive agricultural activities are developed using groundwater [55]. The water needs of agricultural lands are met by groundwater. Aquifer overexploitation, together with the geological characteristics of the area, including thick Quaternary deposits and karstified bedrock, lead to geohazards such as land subsidence and sinkholes. Therefore, sustainable water management and measures to counteract climate change are of great importance in this region.

The basement of the basin consists of three continental blocks: the Sakarya Zone Block, the Kırşehir Massif, and the Torid Block. The Sakarya Zone includes Triassic subduction–accretion complexes overlain by Jurassic–Cretaceous carbonate rocks and Cretaceous–Paleocene volcanic and sedimentary successions [56]. The Kırşehir Massif is characterized by Cretaceous metamorphic and granitic rocks. The Torid Block in the south of the basin consists of Paleozoic–Mesozoic sedimentary rocks. The Eocene sequence includes flysch, limestone, and volcanic rock.

The neo-autochthonous rocks of the basin include Mio–Pliocene terrestrial formations and Miocene–Quaternary volcanic rocks (Figure 4). The Late Miocene–Pliocene İnsuyu Fm. consists of lacustrine micritic limestones, marls, claystones, and sandstones [57,58]. The formation of sinkholes in the Konya Basin is mainly related to the presence of karstified (i.e., cavernous) carbonate rocks of the İnsuyu Fm. Törk et al. (2013) determined a thickness of 180 m for this formation in a borehole drilled near Karapınar. Many cavities with heights  $\geq 50$  cm and reaching up to 190 cm were identified in this borehole, especially concentrated at depths of 24–47, 70–93, and 131–179 m [59]. Canik and Arıgün (2001) presented data from an oil well drilled near Sultanhanı, where the thickness of the İnsuyu Fm. is at least 300 m [60]. The volcanism that occurred in the basin between the middle Miocene and the late Holocene resulted in the widespread distribution of the volcanic rocks, including Miocene andesites, Pliocene Karacadağ volcanites, and Late Holocene maar-related pyroclastic rocks and basalts found near Karapınar and Aksaray in the eastern portion of the basin [58]. Lacustrine and alluvial sediments are interbedded with the volcanic products. Bayarı et al. (2009), using hydrochemical and isotopic data, noted the presence of high contents of dissolved carbon dioxide and volcanic elements in the basin [50]. The volcanic nature of the area has potentially contributed to renewing or enhancing the aggressiveness of the underground waters with respect to carbonate minerals by supplying deep-sourced  $\text{CO}_2$  and  $\text{SO}_2$ , leading to localized hypogene karst [50,60].

Quaternary deposits unconformably overlie the İnsuyu Formation, covering large areas of the basin (Figure 4). The Quaternary cover mainly corresponds to unconsolidated deposits of the Konya paleolake in the Konya–Karapınar sub-basin and the deposits of the Tuz pluvial lake, which covered a much larger area in the Late Pleistocene than today [35,61]. These Quaternary lacustrine sediments, which are up to 400 m thick in places, consist of clays, silts, sands, and gravels with thin evaporite and carbonate layers [58]. The margins of both the Tuz pluvial lake and the Konya pluvial lake are characterized by alluvial fans associated with marginal Quaternary faults. During the Late Pleistocene, climate fluctuations caused water-level changes in the Konya pluvial lake, recorded by four shoreline scarps and lake terraces [62]. There are two generations of nested alluvial fans on the margins of the Konya paleolake, in which base-level changes and tectonic activity

played an important role in their formation [63]. The lake extent peaked during the Last Glacial Maximum, reaching an area of more than 4000 km<sup>2</sup>. Erol (1985) stated that the lake-level changes were instrumental in the formation of the old sinkholes and that they may have controlled the development of caves related to groundwater flow from the Konya paleolake to the relatively low-lying Tuz pluvial lake during the pluvial period [62].

The sub-basins are bounded by faults. The Tuz Gölü sub-basin is bounded by the active NW–SE-trending Tuz Gölü Fault zone, which is one of the main tectonic structures in Central Anatolia [64,65]. This is a right-lateral strike-slip fault with a SW-ward displacement component. The V-shaped Konya graben is one of the largest extensional neotectonic structures in western Anatolia [66]. It is bounded by active normal faults capable of generating large earthquakes (e.g., [67]). The Konya Basin includes a number of smaller intrabasinal grabens and horsts. One of these smaller grabens is the NE–SW-trending Karapınar graben, flanked to the SE by the Karacadağ horst, which is composed of volcanic complexes [66]. The active fault zone bounding the NW margin of the Karapınar graben mainly strikes NE–SW, whereas some segments of the fault show a NW–SSE trend to the north of the graben (e.g., Seyithacı Fault [68]). There are also concealed active normal faults that offset young lacustrine sediments within the basin. The fact that most sinkholes are concentrated close to the faults, forming two main alignments with NE–SW and NW–SSE orientations (Figure 4), reveals strong tectonic control over sinkhole formation [69].

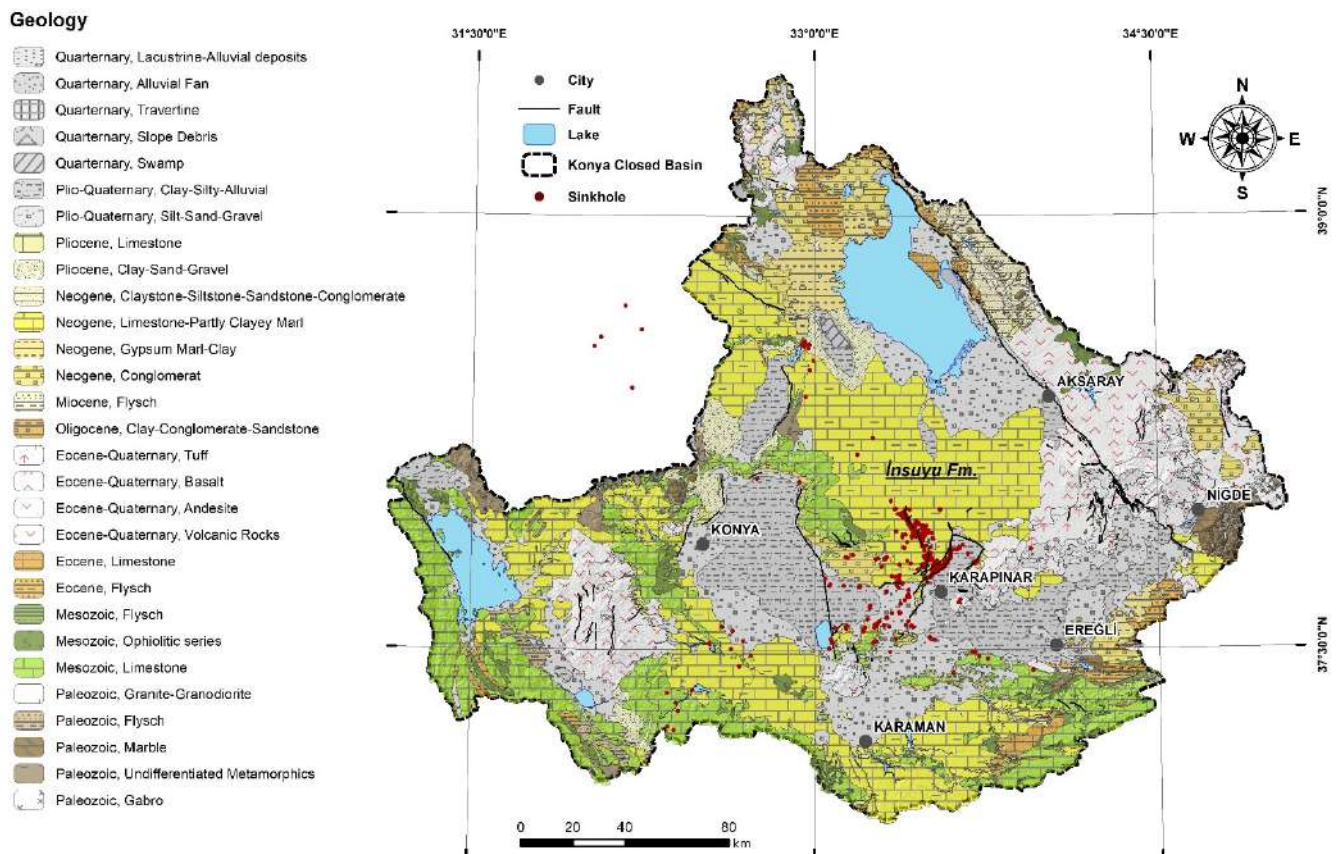


**Figure 4.** Geological map (modified from [70]).

The main groundwater drainage in the Konya endorheic basin has been considered to flow via subsurface channels to Tuz Lake to the NE and via Göksu River to the Mediterranean in the south [3]. Lakes and marshes (e.g., Akgöl) still exist in several sub-basins of the Konya endorheic basin. The surface drainage system from Karaman to Salt Lake seems not to exist anymore, and an underground karst drainage system similar to that of the Taurus Mountains with sinkholes acting as connection pathways has been proposed to exist instead [37,71].

### 3. Data and Methodology

In this study, we used data from various sources to identify the temporal and spatial patterns of land subsidence in the Konya endorheic basin. First, SAR satellite data acquired by Sentinel-1, operated by the European Space Agency, were used to detect ground subsidence in the basin. Groundwater well data showing the temporal variation of the groundwater level were analyzed, and the flow directions in the basin were determined. We analyzed the relationship between land subsidence and the groundwater flow directions in the basin, as well as the drop in the water table level. Sentinel-2 land cover data within the scope of the ESA WorldCover project [72] were also used to reveal the current status of the basin and its relationship with land subsidence. In addition, the cartographic inventory of sinkholes in the region was first provided by the General Directorate of State Hydraulic Works (DSİ) and then updated using georeferenced orthophotos (2021–2022) in a GIS environment. This inventory was refined by field studies, which also included the investigation of surface fissures and scarps associated with land subsidence. This updated sinkhole inventory was used to investigate the spatial distribution of the sinkholes in the basin, their relationship with water table decrease, and its relationship with land subsidence. Finally, the shorelines of the maximum level of the Konya paleolake and the Tuz pluvial lake [36,73] were digitized and used to unravel the relationships of the old shorelines with the deformations in the basin.

#### *InSAR Processing*

To comprehensively analyze surface deformation in the Konya Basin, we employed the InSAR technique using Sentinel-1 data spanning from October 2014 to August 2022. The Konya Basin is covered by two frames (05077 and 05276) of Sentinel-1 data in descending track 167. The LiCSAR automatic InSAR processing platform provided the interferograms were used in this study, with a spatial resolution of approximately 100 by 100 m [74]. In the northern frame (05077), we used a total of 1136 interferograms from 338 Sentinel-1 images. However, it is important to note that a temporal gap exists in the interferogram network between July 2020 and February 2021. Similarly, in the southern frame (05276), we obtained 1218 interferograms from 367 Sentinel-1 images.

To ensure robust surface deformation results, we conducted a small baseline analysis for each frame using the LiCSBAS processor [75]. Tropospheric phase delay correction was applied using Generic Atmospheric Correction Online Service for InSAR (GACOS) products [76]. Additionally, the loop phase was calculated for triplet interferograms to identify and remove interferograms with significant unwrapping errors. Subsequently, 69 and 90 interferograms with large unwrapping errors were eliminated from the northern and southern frames, respectively. The small baseline network inversion was then employed to estimate the deformation time series. To handle the gaps in the interferogram network, we applied a temporal interpolation based on the assumption of a long-term linear deformation.

Next, we masked out pixels that met specific criteria: pixels with more than 10 gaps in the small baseline network, more than 15 unclosed loops, or pixels with a root mean square of residuals in the small baseline inversion higher than 2 mm. After applying the masking process, approximately 89% and 80% of pixels in the northern and southern frames remained, respectively. Subsequently, we applied a low-pass filter in space and a high-pass filter in time to enhance the signal-to-noise ratio and highlight the long-term deformation patterns. Finally, we estimated the average velocity in each frame and stitched the results from both frames to create a seamless velocity map covering the entire Konya Basin. This approach allowed us to obtain a comprehensive and accurate representation of the surface deformation in the study area over the 8-year period from October 2014 to August 2022.

### 4. Results

The SBAS method was used to process Sentinel-1 images taken between October 2014 and August 2022, resulting in a deformation velocity map of the Konya endorheic basin



in the satellite line of sight (LOS) direction (Figure 5). Whereas the red areas in the map represent surface deformation reaching 90 mm/year away from the satellite, the green areas show stable areas in the closed basin where there is no appreciable surface deformation. Subsidence was observed over extensive areas throughout the basin. The spatial extent of land subsidence with LOS rates  $\leq 10$  mm/year covers 7360 km<sup>2</sup>, corresponding to approximately 15% of the closed basin. Given that subsidence is anticipated to be the primary deformation factor in this region, we henceforth refer to the observed deformation away from the satellite as subsidence.

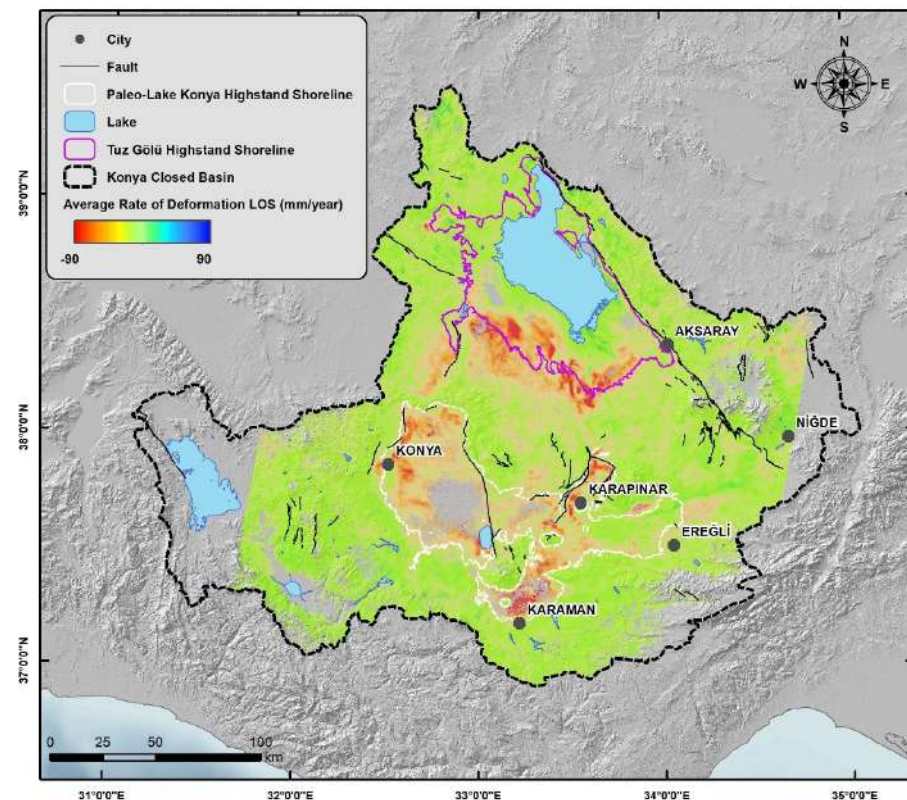


**Figure 5.** Map of average surface deformation rate derived from Sentinel-1 SAR data. Negative values correspond to surface deformation away from the satellite, whereas positive values indicate motion towards the satellite.

Additionally, the surface deformation map in Figure 5 shows the shorelines of the pluvial Tuz Lake and the Konya paleolake within the endorheic basin. It illustrates that the shorelines of the Konya paleolake, shown with white lines, largely coincide with the red areas showing high-rate land subsidence on the deformation map. The main reason for this is the variable facies of the Quaternary sediments accumulated in the paleolake and the uneven consolidation of this material over time, leading to differential subsidence. The pluvial Tuz Lake, located in the northern part of the basin, is shown with pink lines in Figure 5. When the relationship between the pluvial Tuz Lake, which has a surface area of 5800 km<sup>2</sup>, and the InSAR results were examined, it was determined that there was a moderate level of agreement. It is noteworthy that substantial deformation was detected, especially in the southern parts of this lake and outside the border of the pluvial Tuz Lake.

Figures 6 and 7 show land cover, groundwater well locations, InSAR results, and time series of ground subsidence at various settlements and locations within the Konya Basin. As mentioned in the Section 3, the unavailability of interferograms in frame 05077 on the LiCS platform during 2020 and 2021 caused a temporal gap in the time series for points c-III and b-III in Figures 6 and 7, respectively. To address this gap in data coverage, a long-term linear deformation was assumed in the InSAR time series processing. Maps and graphs in Figure 6 illustrate the spatial-temporal variations of ground deformation

in Konya, Karaman, and Aksaray cities and surroundings, as well as their relationships with human factors. The areas in red in Figure 6a-I show the built-up areas in Konya city, whereas those in pink are the croplands. Figure 6a-II shows the ground subsidence values in the same area obtained by the InSAR technique. The comparison of both figures reveals that subsidence zones with LOS rates corresponding to movement away from the satellite greater than 80 mm/y occurred in the central and eastern parts of Konya city. In addition, the time series at the location indicated with a star in Figure 6a-II shows that land subsidence reached 50 cm in LOS in Konya city center in approximately eight years (Figure 6a-III). Rapid subsidence in urban areas, especially when deformation occurs unevenly, can potentially cause significant building damage and economic losses. The effect of subsidence is clearly seen in linear urban elements, such as garden boulevards. In addition, settlement at different rates, which can affect buildings, can cause severe cracking in the structure, compromising its integrity. This situation is commonly observed in doors and windows.

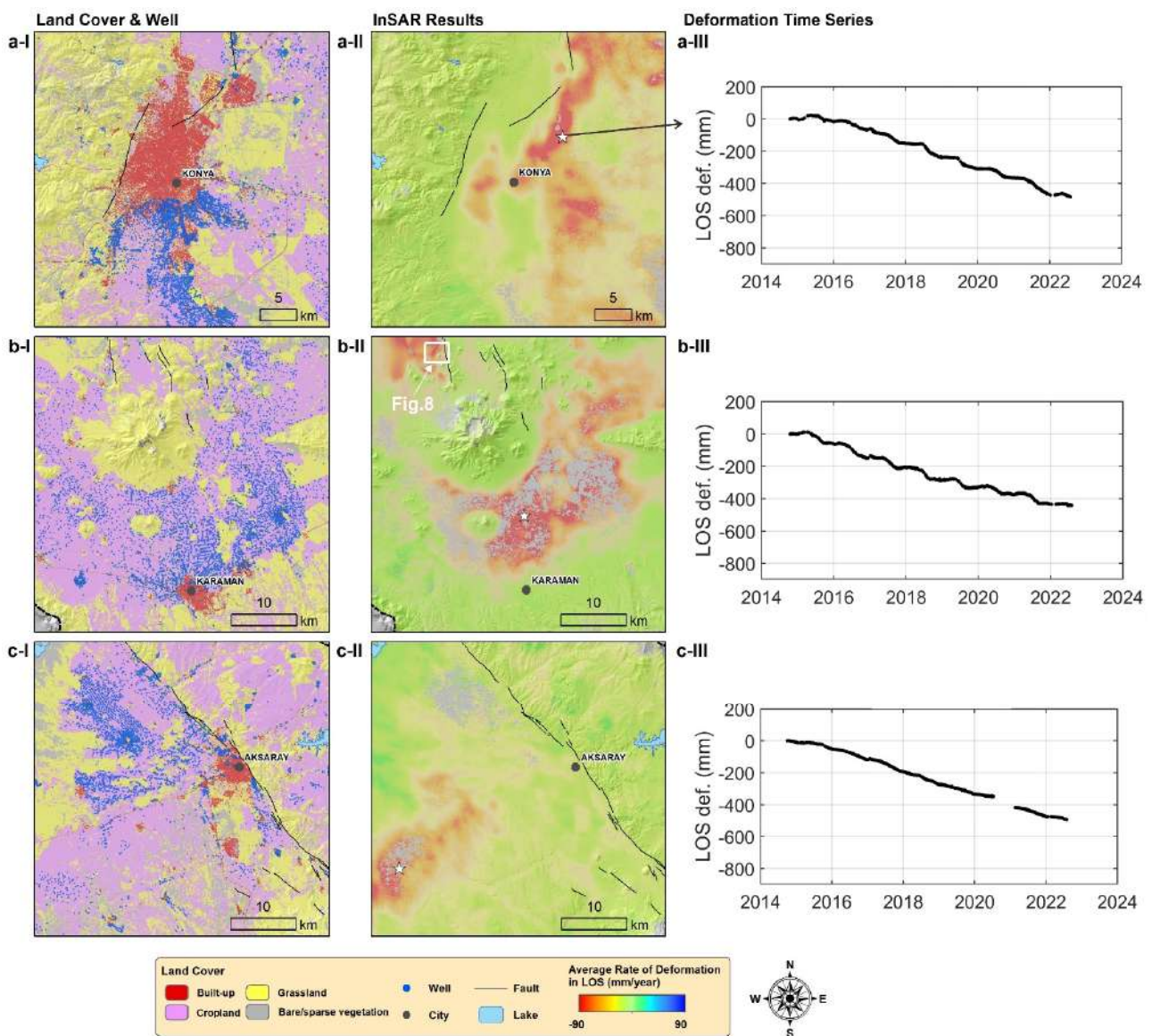


**Figure 6.** Columns designated as (I,II) show the land cover and InSAR results of selected sectors, respectively, and column (III) shows deformation time series at sites indicated with a star in the corresponding displacement maps. Rows (a–c) show results for Konya, Karaman, and Aksaray cities, respectively.



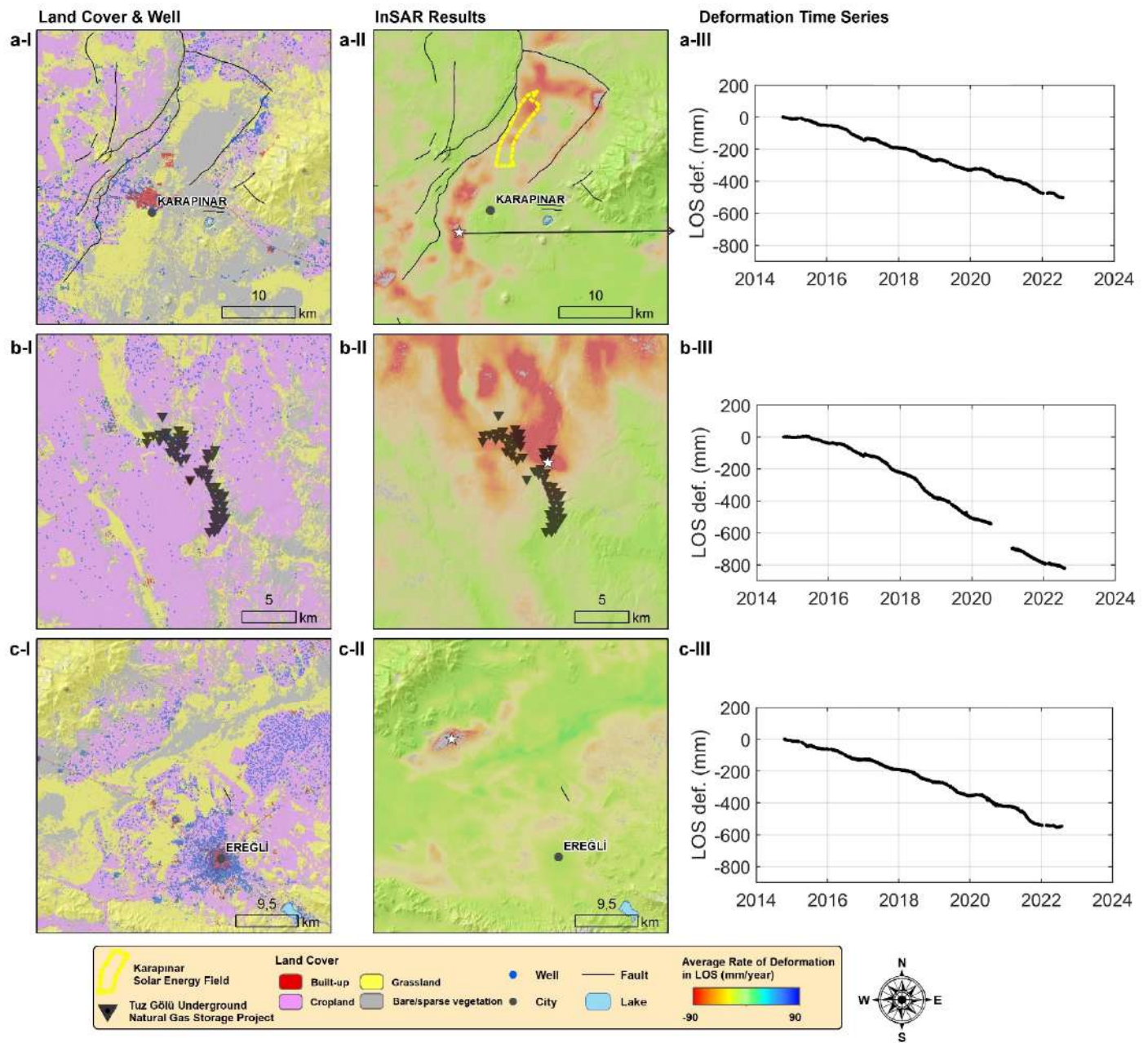


**Figure 7.** Columns designated as (I,II) show the land cover and InSAR results of selected sectors, respectively, and column (III) shows deformation time series at sites indicated with a star in the corresponding displacement maps. Rows (a–c) show results for the Karapınar solar energy field, Tuz Gölü Underground Natural Gas Storage Project, and the Ereğli region, respectively.

In the Karaman area, there was a clear spatial correlation between agricultural areas, wells used for groundwater withdrawal, and areas affected by subsidence (Figure 6b-I,b-II). Since the city center of Karaman is mainly located on bedrock, the subsidence observed in the areas underlain by lake deposits does not occur in the city center of Karaman, founded on bedrock. LOS rates close to  $-80$  mm/y were detected in croplands and grasslands. Additionally, the time series graph of the Karaman region indicates that seasonal water table changes have an effect on deformation values (Figure 6b-III). The time series graph shows that although deformation slows down in the winter months, subsidence rates increase in the summer months due to the water table drop. Intensive agricultural activities are carried out in the Aksaray city area, like in other sectors of the basin. At the same time, the



NW–SE-oriented Tuz Gölü Fault zone runs along the NE edge of the city (Figure 6c-I,c-II). InSAR results indicate LoS rates between  $-10$  mm/y and  $-70$  mm/y, especially in the downthrown block of the fault (i.e., basin fill), whereas no deformation was identified in the bedrock terrain of the footwall. Additionally, slow subsidence was detected in Aksaray city center.

In the Karapınar region, where approximately 90% of the recent sinkholes have formed, no deformation was observed in the city or the eastern parts, whereas LOS rates reaching  $-60$  mm/y were observed in the western parts (Figure 7a-II). LOS deformation values of up to  $-75$  mm/year were observed in croplands and some grasslands, as shown in Figure 7a-I. In addition, the spatial distribution of ground subsidence in the Karapınar region is restricted by faults, which define the boundary of the unconsolidated deposits of the basin fill. The Karapınar solar power plant, which is the largest in Europe and one of the largest solar plants in the world, is located in the endorheic basin. This renewable energy facility, covering an area equivalent to about 2600 soccer fields, was built with an investment of USD 1 billion. According to the InSAR results in the area, framed by a dashed yellow line in Figure 7a-II, a significant portion of this land is affected by subsidence that might cause damage. LOS rates as high as  $-60$  mm/year were observed in this area. Additionally, the facility is located in the vicinity of a sinkhole area with a high probability of new sinkhole occurrence. Therefore, this area is also threatened by potential sinkhole damage. Another region within the basin that is strategically important and can be considered hazardous is the Tuz Gölü Underground Natural Gas Storage Project area, located in the southern parts of Tuz Lake. The places shown with black triangles in Figure 7b-I show the approximate locations of this natural gas storage area. This region is where the highest subsidence values were observed in the basin, with LOS rate values as high as  $-100$  mm/y. InSAR results and land cover maps of the Ereğli region are shown in Figure 7c-I,c-III, respectively. While no subsidence is observed in the Ereğli city center, underground by bedrock similar to Karaman city, LOS deformation rates of up to  $-75$  mm/y was observed in places with intense agricultural activities.

Figure 8b shows an image taken from an unmanned aerial vehicle and topographic/deformation profiles of the N–S-oriented surface fissures and scarps examined in the Adakale/Karapınar region in August 2023. This site is associated with the eastern margin of the Konya Lake graben, controlled by a N–S-striking and west-dipping normal fault system, whose main strand runs next to Adakale village. The topographic profile traverses a 120 m-high andesite hill in the east, and the piedmont to the west is underlain by basin-fill alluvium. These scarps–fissures, which are up to 500 m long, are parallel to the basin margin fault and show a westward vertical displacement of up to 2 m, consistent with the normal fault system that controls the margin of the graben and thickness variations in the basin fill (Figure 8b). InSAR data indicate that land subsidence is restricted to the area underlain by alluvium, reaching values of  $-80$  mm/y in LOS, whereas no displacement was recorded on the hill with exposed bedrock. These surface ruptures are compatible with differential compaction controlled by sharp lateral changes in the overburden thickness, likely governed by concealed normal westward faults.

In order to analyze the spatial and temporal patterns of land subsidence, the subsidence map of the study area, the land cover map of 2021, the temporal variations in groundwater levels, and possible groundwater flow directions were determined and are shown in Figures 9–11. ESA land cover data from 2021 were used to assess the spatial relationship between the current land use and the two types of subsidence—mainly large-scale subsidence detected by InSAR plus cover collapse sinkholes. The Konya endorheic basin consists of 41.6% (20,700 km<sup>2</sup>) cropland, 39.5% (19,657 km<sup>2</sup>) grassland, 9.7% (4843 km<sup>2</sup>) bare/sparse vegetation, 3.8% (1923 km<sup>2</sup>) tree cover, 3.7% (1856 km<sup>2</sup>) permanent water bodies, and 1.5% (750 km<sup>2</sup>) built-up areas. Less than 1% consists of herbaceous wetlands and shrublands (Figure 9). When the land cover in which the recent sinkholes occurred were analyzed, it was determined that 390 (60%) of the sinkholes formed in grasslands, 195 (30%) in croplands, 73 (11%) in bare/sparse vegetation areas, and 2 in built-up areas.

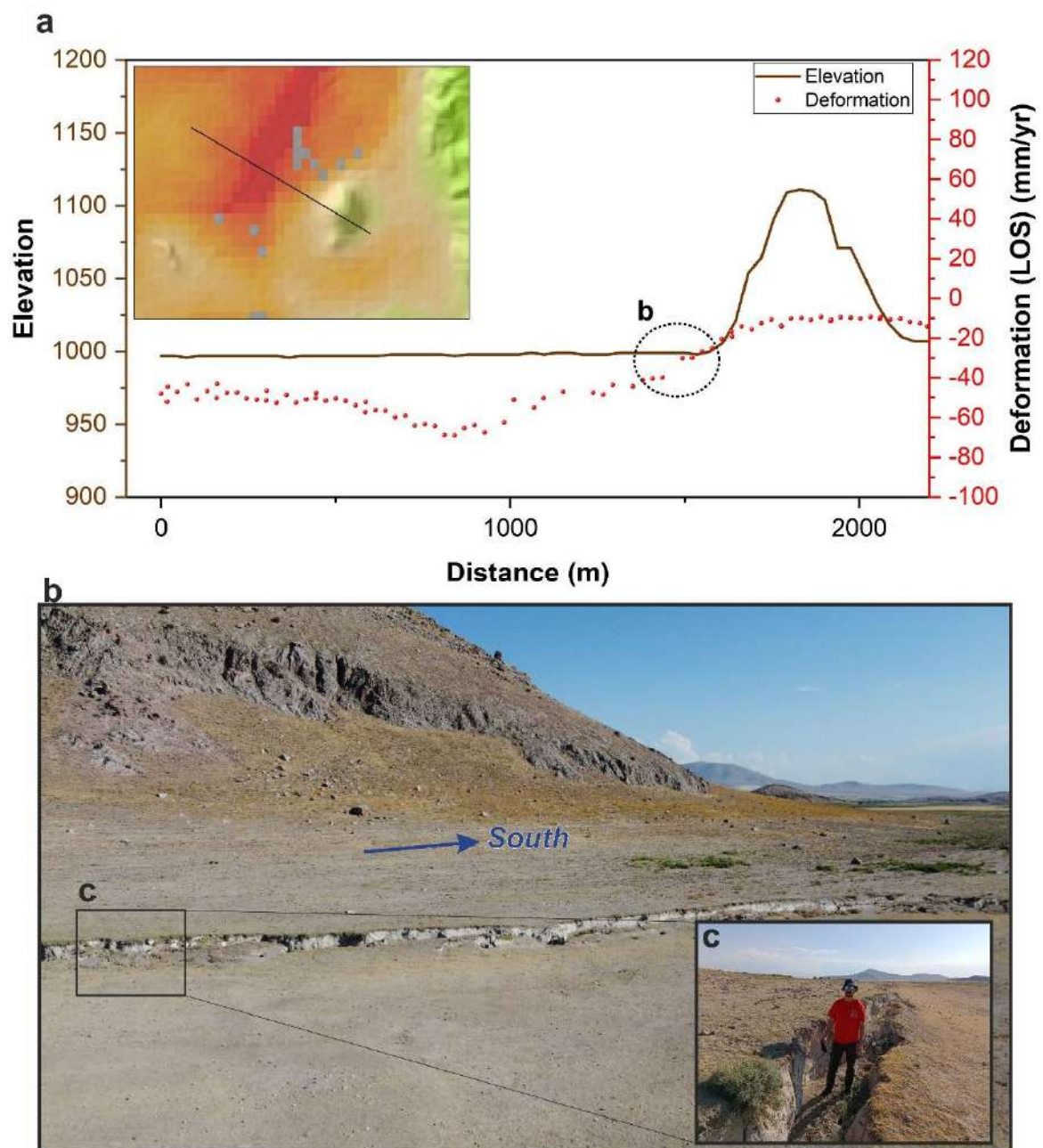


**Figure 8.** (a) Profiles showing the topography in a section perpendicular to the west-facing scarps–fissures alongside displacement rates (check Figure 6 for deformation legend). (b) Images of the N–S-oriented and westward scarps–fissures formed in the Adakale/Karapınar region. (c) Image indicating the depth of the surface fissures and the deformation. Note the vertical downward displacement on the right (west) side of the fissure–scarp. View looking south.

On the other hand, the relationships between land subsidence and sinkhole formations observed in the endorheic basin with groundwater withdrawals and groundwater table were examined temporally and spatially. Figure 9 shows that the areas affected by higher subsidence rates tended to be associated with the shorelines of the pluvial Konya and Tuz lakes, as documented in the literature [6,73]. Figure 10 shows groundwater level changes between 2022–2000 and 2022–2014. Although the average decrease was around 20 m between 2000 and 2014, it was determined that water table drop increased to 40 m in 2022. In addition, the regions where sinkholes are most common correspond to areas with the greatest groundwater level decreases. Figure 10 shows the overall groundwater-level

change in the study area using 30 observation wells with long-term and continuous data. Although the maximum water level depth in the region was 72.88 m in 2000, it was 85.66 m in 2014 and 96.86 m in 2022. The average groundwater level depth of the 30 observation wells was 23.63, 31.47, and 39.45 m for 2000, 2014, and 2022, respectively. Thus, it can be estimated that the average water table decrease in the region was 0.69 m/y. Figure 11 also depicts the possible groundwater flow directions based on contour lines of the groundwater level (i.e., equipotential lines). Groundwater flows northwards from the Taurus foothills to the central areas and then towards Lake Tuz, located in the north of the basin and functioning at the regional base level (Figure 11) [6].

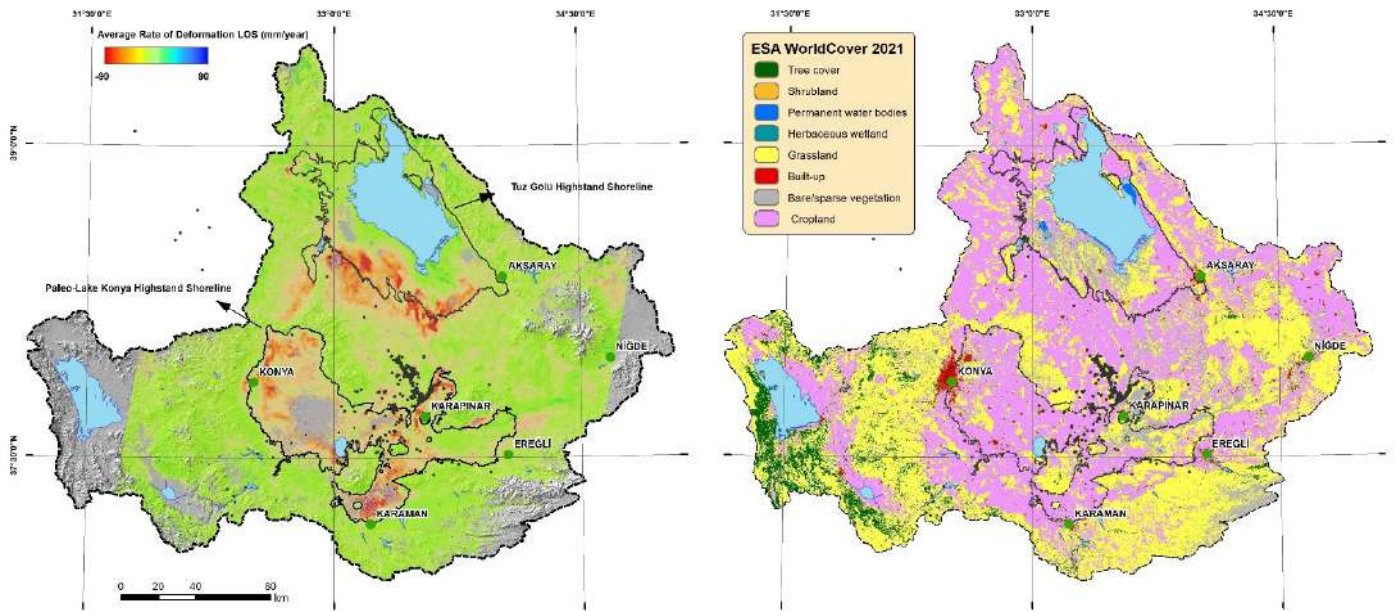


Figure 9. Left: land subsidence map of Konya Closed Basin. Right: 2021 land cover map of the basin.

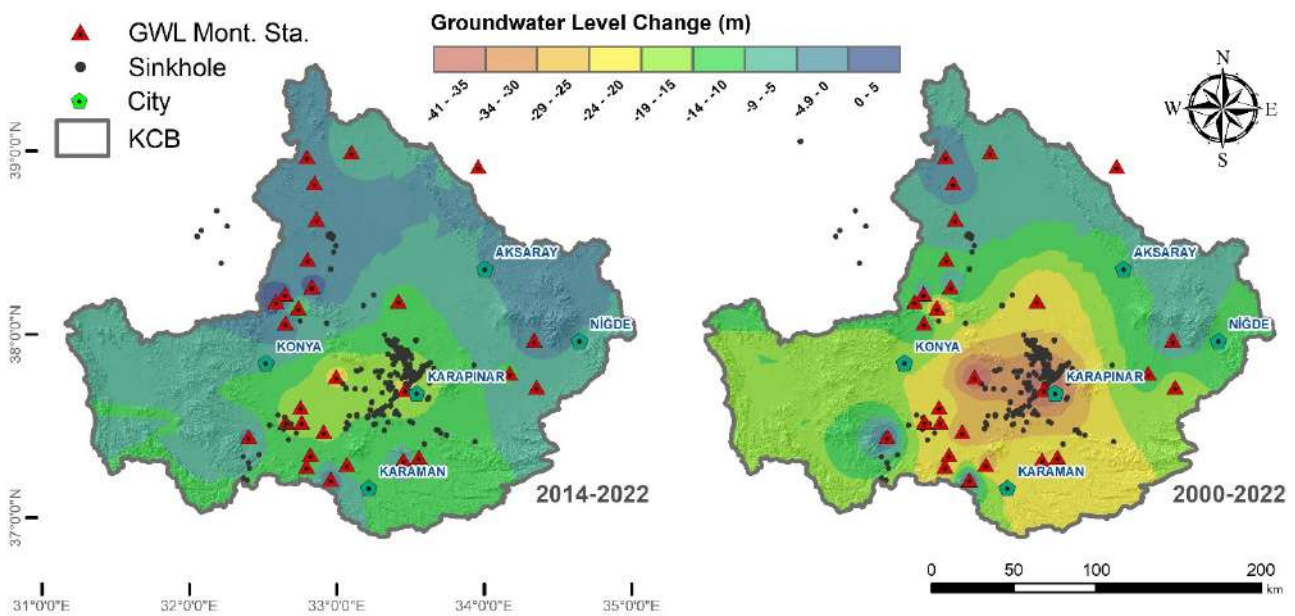
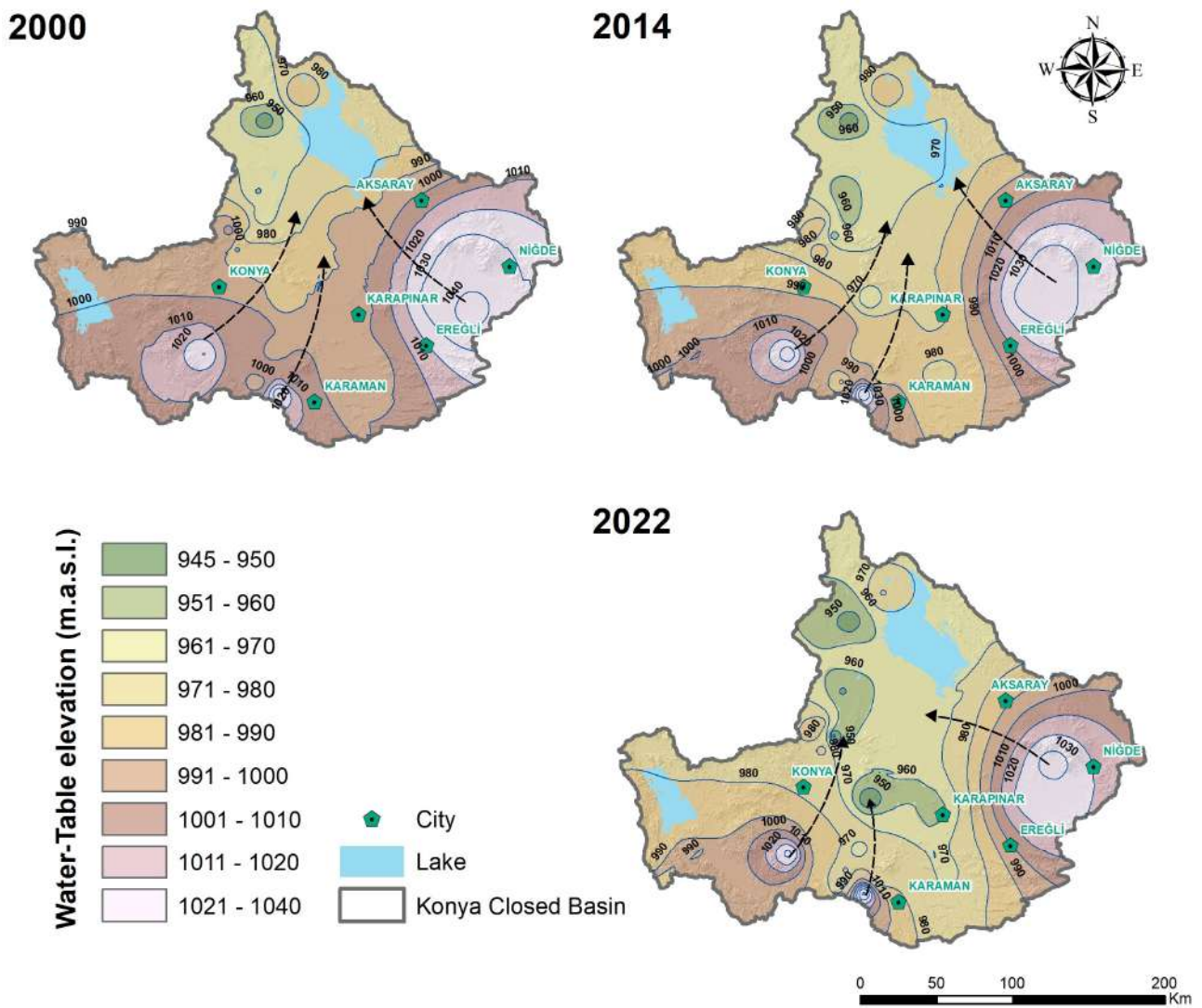


Figure 10. Groundwater-level drop that occurred over the periods 2014–2022 and 2000–2022.





**Figure 11.** Groundwater elevation and possible flow directions in Konya Closed Basin.

### 5. Discussion

This study analyzes land subsidence induced by groundwater over-pumping in the Konya endorheic basin using (1) InSAR displacement data (deformation maps and time series) derived from Sentinel-1 data covering the period 2014–2022, (2) spatial–temporal variations of groundwater level, (3) land cover data, and (4) field studies. Land subsidence locally reached satellite LOS rates of 90–100 mm/y between 2014 and 2022.

Previously published information in areas such as Konya [51,77], Karaman [78], and Karapınar [79] was updated and refined in this study. Moreover, active land subsidence in the Aksaray, Ereğli, and Niğde settlements and their surroundings were investigated for the first time. In addition, the land subsidence in the Tuz Gölü Underground Natural Gas Storage Project area and the Karapınar solar power plant area, which are economically and strategically important regions, were investigated. It was observed that these strategically important areas suffer from rapid ground subsidence, which may potentially cause damage to these facilities. In 2012, a sinkhole with a diameter of approximately 110 m formed in Louisiana in the USA [80]. When the reasons for the formation of this sinkhole were investigated, it was reported that it was caused by emptied salt domes operated by the Texas Brine Company in the region and opened for underground gas storage [80]. All settlements near this sinkhole, called the Bayou Corne sinkhole, were evacuated, and economic losses were experienced in the region [81]. Other areas of sinkhole and subsidence formation above

solution salt mining include Pinheiro (Maceió), Brazil [82], where even after a complete stop to salt mining, the area continues to subside, and recently, a submerged sinkhole appeared. Also, the famous Cerville–Buissoncourt salt-mining sinkhole in France [83] is an important case study for triggered large-scale collapses. Therefore, Salt Lake Underground Natural Gas Storage authorities should consider such situations and use monitoring systems for surface deformations.

The main reasons for the occurrence of severe instances of land subsidence are (1) the over-exploitation of aquifers for agricultural activities and the accompanying groundwater-level drop; (2) natural basin fill, including thick fine-grained deposits subject to progressively higher normal effective stresses beyond the pre-consolidation stress; and (3) the semiarid climate of the region, which contributes to increasing water demands in crops and restricts groundwater recharge in the endorheic basin. Previous studies conducted by [51,79] document that the region turned to intensive irrigated agricultural activities especially after the 2000s and that the majority of groundwater wells used for irrigation needs in the region have been performed without permission. Moreover, our field studies and interviews with farmers indicate that irrigated agricultural activities continue to increase in the basin and that new illegal wells continue to be developed.

Concealed normal faults most likely control sharp variations in the thickness of the lacustrine and alluvial deposits of the basin fill. Greater cumulative consolidation–compaction in the thicker sediments on the downthrown side of the faults may result in differential subsidence with abrupt lateral gradient changes across the faults. This may result in the development of non-tectonic scarps and fissures (Figures 2c and 8), as documented in other basins where the water table has decreased (e.g., [84]). Therefore, basin margins close to fault systems are more prone to differential subsidence and the formation of potentially damaging ground ruptures.

Points #1 and #2 shown in Figure 12 are located in Konya city, where approximately 2 million people live. According to the InSAR results, point #1 experienced rapid subsidence at an LOS rate of approximately  $-60$  mm/y between 2014 and 2018, whereas a lower rate of  $-10$  to  $-15$  mm/year was observed between 2018 and 2022 (Figure 12a). Figure 12a shows the groundwater level of a well near the city center. The groundwater-level data show that water usage exceeded the recovery capability of the aquifer by recharge until 2018, and the deformation value increased over time in direct proportion to the decline in the water level. Between 2018 and 2022, the amount of groundwater withdrawal decreased and subsidence slowed down accordingly. Şireci et al. (2021) observed a decrease in the subsidence rate in this region after 2018 approximately at the location of point #1 [77]. Thus, the result of this study is in good agreement with their study. Figure 12b shows the InSAR results at point #2 in the northeastern part of Konya city. The displacement time series of this point, shown with red lines, shows the subsidence of the western part of the city, which reached 550 mm in LOS between 2014 and 2022. When the groundwater-level data of well no. 181 was examined, it clearly showed a constant declining trend, which is one of the main reasons for land subsidence and the occurrence of recent cover collapse sinkholes in the basin. There is a strong correlation between the InSAR time series and the groundwater table levels in wells on the alluvium, indicating that the region's subsidence is caused by over-exploitation of aquifers, as documented by [51,77,79,85].

Differential land subsidence can cause damage to linear structures (highways, railways, water networks, pipelines, flood-control structures, and sewer lines) [86]. For example, in regions of Arizona, more than 500 times the amount of naturally replenished groundwater has been used for irrigation, mining, and utilities since 1900 [87]. The resulting groundwater-level decreases have caused increased pumping costs in some places, decreased groundwater quality in many places and damaging linear objects [88]. In order to eliminate or minimize the damage, it is necessary to control groundwater withdrawal and prevent or minimize the decrease in groundwater level.

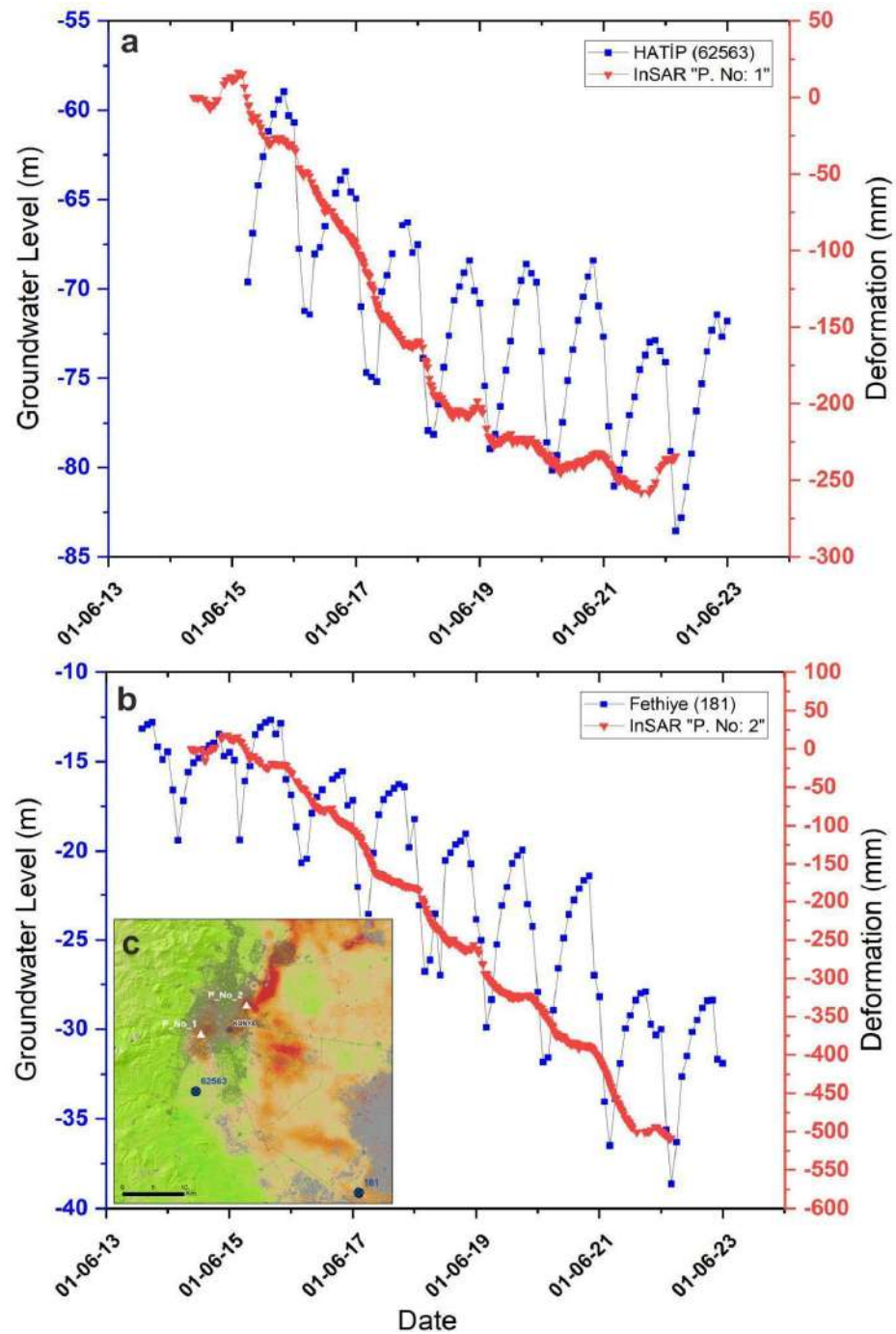


**Figure 12.** LOS deformation time series of the eastern and western sectors of Konya city (red lines). Graphs of the temporal variation in groundwater level at Hatip (a) and Fethiye (b) stations (blue lines). Note the seasonal variations superimposed on the general decreasing trend. (c) The white triangles represent subsidence points and the blue circles represent groundwater wells.

The groundwater-level drop, which occurred at a rate of around 0.5 m/y before the 2000s, has reached a current average of 8 m/y. Agricultural crops with high water demand such as sugar beet and corn impose an unsustainable impact on the aquifers, with limited recharge given the semiarid climate of the region. A transition towards crops with less or null irrigation water demand would significantly contribute to mitigating the subsidence hazards induced by groundwater over-exploitation.



## 6. Conclusions

The Konya endorheic basin in Central Anatolia Region, Türkiye, where 3 million people live, has various important assets, such as extensive agriculture, ecosystem diversity, and animal husbandry. This endorheic basin has ideal conditions for growing dry agricultural products such as wheat, barley, and cotton. However, in the last two decades, a profound transformation has been carried out on irrigated agriculture that is incompatible with the region's climatic conditions and hydrology. This transformation, together with urban development, have caused excessive groundwater withdrawal, leading to a continuous decline in the groundwater level. This human-induced change in the hydrology has caused land subsidence, local surface ruptures (scarps and fissures), and sinkhole formation in the endorheic basin, as has recently been observed in many regions.

Within the scope of this study, the temporal and spatial patterns of land subsidence in the Konya Basin were successfully determined using the InSAR technique. The obtained ground deformation was compared with paleolake highstand shorelines, land cover data, and groundwater data, with consistent relationships being observed. Aquifer overexploitation due to erroneous agricultural policies causes the depletion of aquifer systems and triggers sinkhole formation and surface deformation of as much as 90–100 mm/y away from the satellite, corresponding to land subsidence. In addition, the presence of strategic facilities of great economic importance makes this region particularly sensitive to human-induced hazards. Therefore, it is critical to design and implement sustainable agricultural plans and raise awareness among farmers about these issues. We estimate that there are currently 100,000 illegal wells in the region. It would be desirable to restrict and control these wells with practices such as quota applications.

This study has demonstrated how Sentinel-1 satellite data can be an effective tool for quantitatively determining the temporal and spatial extent of land subsidence in a large study area. Moreover, critical issues related to managing groundwater resources, land subsidence, ground fissures, and sinkhole formation can be tackled in other parts of the world by using the approaches applied in this study.

**Author Contributions:** O.O.: fiction, data, application, fieldwork, article writing, and revision; M.H.H.: data, application, manuscript writing, and revision; V.D.: data, hydrology interpretation, field work, manuscript writing, and revision; E.G.: geological interpretation, fieldwork, article writing, and revision; F.G.: advisor, fieldwork, article writing, and revision, D.A.-H.: fiction, data, article writing, and revision. All authors have read and agreed to the published version of the manuscript.

**Funding:** This research received no external funding.

**Data Availability Statement:** For reasonable collaborative studies, data used in the study are available from the authors.

**Acknowledgments:** The authors would like to thank the State Hydraulic Works and its employees for the data they shared and the General Directorate of Mapping and Konya Metropolitan Municipality for the orthophotos. The authors also would like to thank Daniel Melnick for providing paleoshoreline data. LiCSAR contains modified Copernicus Sentinel data 2014–2023 analysed by the Centre for the Observation and Modelling of Earthquakes, Volcanoes and Tectonics (COMET). LiCSAR uses JASMIN, the UK's collaborative data analysis environment (<http://jasmin.ac.uk>, accessed on 19 December 2023). This study is the extended version of the abstract titled "Investigation of the land subsidence in the Konya Closed Basin, Turkey", presented at the 3rd MedGU-23, İstanbul.

**Conflicts of Interest:** The authors declare no conflicts of interest.

## References

1. Ford, D.; Williams, P. *Karst Hydrogeology and Geomorphology*; Wiley: Chichester, UK, 2007; ISBN 9780470849965.
2. De Waele, J.; Gutiérrez, F. *Karst Hydrogeology, Geomorphology and Caves*; Wiley: Hoboken, NJ, USA, 2022; ISBN 9781119605348.
3. Nazik, L.; Poyraz, M.; Karabiyıkoğlu, M. Landscapes and Landforms of Turkey. In *World Geomorphological Landscapes—Karst Landscapes and Landforms in Turkey*; Kuzucuoğlu, C., Çiner, A., Kazancı, N., Eds.; World Geomorphological Landscapes; Springer Nature: Cham, Switzerland, 2019; ISBN 978-3-030-03513-6.

4. Şengör, A.M.C.; Görür, N.; Şaroğlu, F. *Strike-Slip Faulting and Related Basin Formation in Zones of Tectonic Escape: Turkey as a Case Study*; SEPM Society for Sedimentary Geology: Claremore, OK, USA, 1985.
5. Gürbüz, A.; Kazancı, N. Genetic Framework of Neogene-Quaternary Basin Closure Process in Central Turkey. *Lithosphere* **2015**, *7*, 421–426. [[CrossRef](#)]
6. Melnick, D.; Yıldırım, C.; Hillemann, C.; Garcin, Y.; Çiner, A.; Pérez-Gussinyé, M.; Strecker, M.R. Slip along the Sultanhanı Fault in Central Anatolia from Deformed Pleistocene Shorelines of Palaeo-Lake Konya and Implications for Seismic Hazards in Low-Strain Regions. *Geophys. J. Int.* **2017**, *209*, 1431–1454. [[CrossRef](#)]
7. Nagehan Ucan, H.; Dursun, S. Environmental Problems of Tuz Lake (Konya-Turkey). *J. Int. Environ. Appl. Sci.* **2009**, *4*, 231–233.
8. Aydın, F.; Erat, E.; Türkeş, M. Impact of Climate Variability on the Surface of Lake Tuz (Turkey), 1985–2016. *Reg. Environ. Chang.* **2020**, *20*, 68. [[CrossRef](#)]
9. Nazik, L.; Tuncer, K. Regional Features of Turkish Karst Morphology. *Turk. J. Speleol. Karst Cave Res.* **2010**, *1*, 7–19.
10. Tudryn, A.; Motavalli-Anbaran, S.H.; Tucholka, P.; Gibert-Brunet, E.; Lankarani, M.; Ahmady-Birgani, H.; Kong, T.; Noret, A.; Miska, S.; Massault, M.; et al. Late Quaternary Environmental Changes of Lake Urmia Basin (NW Iran) Inferred from Sedimentological and Magnetic Records. *Quat. Int.* **2021**, *589*, 83–94. [[CrossRef](#)]
11. Vey, S.; Al-Halbouni, D.; Haghshenas, M.; Alshawaf, F.; Vüllers, J.; Güntner, A.; Dick, G.; Ramatschi, M.; Teatini, P.; Wickert, J.; et al. Delayed Subsidence of the Dead Sea Shore Due to Hydro-Meteorological Changes. *Sci. Rep.* **2021**, *11*, 13518. [[CrossRef](#)] [[PubMed](#)]
12. Hansen, K. NASA Disappearing Lake Tuz. Available online: <https://earthobservatory.nasa.gov/images/149211/disappearing-lake-tuz> (accessed on 1 December 2023).
13. Kilic, O.; Kilic, A.M. Salt Crust Mineralogy and Geochemical Evolution of the Salt Lake (Tuz Gölü), Turkey. *Sci. Res. Essays* **2010**, *5*, 1317–1324.
14. Demir, V. Trend Analysis of Lakes and Sinkholes in the Konya Closed Basin, in Turkey. *Nat. Hazards* **2022**, *112*, 2873–2912. [[CrossRef](#)]
15. Orhan, O.; Yakar, M.; Ekercin, S. An Application on Sinkhole Susceptibility Mapping by Integrating Remote Sensing and Geographic Information Systems. *Arab. J. Geosci.* **2020**, *13*, 886. [[CrossRef](#)]
16. Al-Halbouni, D.; Holohan, E.P.; Saberi, L.; Alrshdan, H.; Sawarieh, A.; Closson, D.; Walter, T.R.; Dahm, T. Sinkholes, Subsidence and Subrosion on the Eastern Shore of the Dead Sea as Revealed by a Close-Range Photogrammetric Survey. *Geomorphology* **2017**, *285*, 305–324. [[CrossRef](#)]
17. Nikraftar, Z.; Parizi, E.; Hosseini, S.M.; Ataie-Ashtiani, B. Lake Urmia Restoration Success Story: A Natural Trend or a Planned Remedy? *J. Great Lakes Res.* **2021**, *47*, 955–969. [[CrossRef](#)]
18. Scheidt, J.; Lerche, I.; Paleologos, E.K. Environmental and Economic Risks from Sinkholes in West-Central Florida. *Environ. Geosci.* **2005**, *12*, 207–217. [[CrossRef](#)]
19. Festa, V.; Fiore, A.; Parise, M.; Siniscalchi, A. Sinkhole Evolution in the Apulian Karst of Southern Italy: A Case Study, with Some Considerations on Sinkhole Hazards. *J. Cave Karst Stud.* **2012**, *74*, 137–147. [[CrossRef](#)]
20. Jiang, H.; Balz, T.; Li, J.; Mishra, V. Preliminary Investigation of Sudden Ground Subsidence and Building Tilt in Balitai Town, Tianjin City, on 31 May 2023. *Remote Sens.* **2023**, *15*, 4891. [[CrossRef](#)]
21. Kim, J.-W.; Lu, Z.; Degrandpre, K. Ongoing Deformation of Sinkholes in Wink, Texas, Observed by Time-Series Sentinel-1A SAR Interferometry (Preliminary Results). *Remote Sens.* **2016**, *8*, 313. [[CrossRef](#)]
22. Gao, Y.; Alexander, E.C. Sinkhole Hazard Assessment in Minnesota Using a Decision Tree Model. *Environ. Geol.* **2008**, *54*, 945–956. [[CrossRef](#)]
23. Goodbar, A.; Powers, D.; Goodbar, J.; Holt, R. Karst and Sinkholes at Nash Draw, Southeastern New Mexico (USA). In Proceedings of the 16th Multidisciplinary Conference on Sinkholes and the Engineering and Environmental Impacts of Karst, San Juan, Puerto Rico, 20–24 April 2020; National Cave and Karst Research Institute: Carlsbad, NM, USA, 2020.
24. Kaufmann, O.; Quinif, Y. Geohazard Map of Cover-Collapse Sinkholes in the “Tournaisis” Area, Southern Belgium. *Eng. Geol.* **2002**, *65*, 117–124. [[CrossRef](#)]
25. Margiotta, S.; Marini, G.; Fay, S.; D’Onghia, F.M.; Liso, I.S.; Parise, M.; Pinna, M. Hydro-Stratigraphic Conditions and Human Activity Leading to Development of a Sinkhole Cluster in a Mediterranean Water Ecosystem. *Hydrology* **2021**, *8*, 111. [[CrossRef](#)]
26. Guarino, P.M.; Nisio, S. Anthropogenic Sinkholes in the Territory of the City of Naples (Southern Italy). *Phys. Chem. Earth* **2012**, *49*, 92–102. [[CrossRef](#)]
27. Galve, J.P.; Gutiérrez, F.; Lucha, P.; Bonachea, J.; Remondo, J.; Cendrero, A.; Gutiérrez, M.; Gimeno, M.J.; Pardo, G.; Sánchez, J.A. Sinkholes in the Salt-Bearing Evaporite Karst of the Ebro River Valley Upstream of Zaragoza City (NE Spain). Geomorphological Mapping and Analysis as a Basis for Risk Management. *Geomorphology* **2009**, *108*, 145–158. [[CrossRef](#)]
28. Nof, R.N.; Abelson, M.; Raz, E.; Magen, Y.; Atzori, S.; Salvi, S.; Baer, G. SAR Interferometry for Sinkhole Early Warning and Susceptibility Assessment along the Dead Sea, Israel. *Remote Sens.* **2019**, *11*, 89. [[CrossRef](#)]
29. Al-Halbouni, D.; AlRabayah, O.; Nakath, D.; Rüpke, L. A Vision on a UNESCO Global Geopark at the Southeastern Dead Sea in Jordan—How Natural Hazards May Offer Geotourism Opportunities. *Land* **2022**, *11*, 553. [[CrossRef](#)]
30. Taheri, K.; Gutiérrez, F.; Mohseni, H.; Raeisi, E.; Taheri, M. Sinkhole Susceptibility Mapping Using the Analytical Hierarchy Process (AHP) and Magnitude–Frequency Relationships: A Case Study in Hamadan Province, Iran. *Geomorphology* **2015**, *234*, 64–79. [[CrossRef](#)]

31. Gökkaya, E.; Gutiérrez, F. Poljes in the Sivas Gypsum Karst, Turkey. *Geomorphology* **2022**, *417*, 108451. [[CrossRef](#)]
32. Ozdemir, A. Sinkhole Susceptibility Mapping Using Logistic Regression in Karapınar (Konya, Turkey). *Bull. Eng. Geol. Environ.* **2016**, *75*, 681–707. [[CrossRef](#)]
33. Orhan, O.; Oliver-Cabrera, T.; Wdowinski, S.; Yalvac, S.; Yakar, M. Land Subsidence and Its Relations with Sinkhole Activity in Karapınar Region, Turkey: A Multi-Sensor InSAR Time Series Study. *Sensors* **2021**, *21*, 774. [[CrossRef](#)]
34. Gutiérrez, F. Sinkhole Hazards. In *Oxford Research Encyclopedia of Natural Hazard Science*; Oxford University Press: Oxford, UK, 2016.
35. Kashima, K. Environmental and Climatic Changes during the Last 20,000 Years at Lake Tuz, Central Turkey. *CATENA* **2002**, *48*, 3–20. [[CrossRef](#)]
36. Roberts, N. Age, Palaeoenvironments, and Climatic Significance of Late Pleistocene Konya Lake, Turkey. *Quat. Res.* **1983**, *19*, 154–171. [[CrossRef](#)]
37. Kuzucuoglu, C.; Parish, R.; Karabiyikoglu, M. The Dune Systems of the Konya Plain (Turkey): Their Relation to Environmental Changes in Central Anatolia during the Late Pleistocene and Holocene. *Geomorphology* **1998**, *23*, 257–271. [[CrossRef](#)]
38. Dursun, A.E. Risk Analysis of Natural Sinkholes Hazards in Karapınar Basin (Konya, Turkey). *Arab. J. Geosci.* **2022**, *15*, 279. [[CrossRef](#)]
39. Ozdemir, A. Investigation of Sinkholes Spatial Distribution Using the Weights of Evidence Method and GIS in the Vicinity of Karapınar (Konya, Turkey). *Geomorphology* **2015**, *245*, 40–50. [[CrossRef](#)]
40. Günay, G.; Çörekçiöğlü, I.; Övül, G. Geologic and Hydrogeologic Factors Affecting Sinkhole (Obruk) Development in Central Turkey. *Carbonates Evaporites* **2011**, *26*, 3–9. [[CrossRef](#)]
41. Doğan, U.; Yılmaz, M. Natural and Induced Sinkholes of the Obruk Plateau and Karapidotlessnar-Hotamiş Plain, Turkey. *J. Asian Earth Sci.* **2011**, *40*, 496–508. [[CrossRef](#)]
42. Waltham, T. Large Collapse Sinkholes, Old and New, in the Obruk Plateau, Turkey. *Cave Karst Sci.* **2015**, *42*, 125–130.
43. Watson, R.A.; Holohan, E.P.; Al-Halbouni, D.; Saberi, L.; Sawarieh, A.; Closson, D.; Alrshdan, H.; Abou Karaki, N.; Siebert, C.; Walter, T.R.; et al. Sinkholes and Uvalas in Evaporite Karst: Spatio-Temporal Development with Links to Base-Level Fall on the Eastern Shore of the Dead Sea. *Solid Earth* **2019**, *10*, 1451–1468. [[CrossRef](#)]
44. Sevil, J.; Gutiérrez, F. Morphometry and Evolution of Sinkholes on the Western Shore of the Dead Sea. Implications for Susceptibility Assessment. *Geomorphology* **2023**, *434*, 108732. [[CrossRef](#)]
45. Wadas, S.H.; Buness, H.; Rochlitz, R.; Skiba, P.; Günther, T.; Grinat, M.; Tanner, D.C.; Polom, U.; Gabriel, G.; Krawczyk, C.M. Geophysical Analysis of an Area Affected by Subsurface Dissolution—Case Study of an Inland Salt Marsh in Northern Thuringia, Germany. *Solid Earth* **2022**, *13*, 1673–1696. [[CrossRef](#)]
46. Pasvanoğlu, S.; Güner, A.; Gültekin, F. Environmental Problems at the Nevşehir (Kozakli) Geothermal Field, Central Turkey. *Environ. Earth Sci.* **2012**, *66*, 549–560. [[CrossRef](#)]
47. Hermosilla, R.G. The Guatemala City Sinkhole Collapses. *Carbonates Evaporites* **2012**, *27*, 103–107. [[CrossRef](#)]
48. Sandhu, D.; Singh, A.; Duranceau, S.J.; Nam, B.H.; Mayo, T.; Wang, D. Fate and Transport of Radioactive Gypsum Stack Water Entering the Floridan Aquifer Due to a Sinkhole Collapse. *Sci. Rep.* **2018**, *8*, 11439. [[CrossRef](#)] [[PubMed](#)]
49. Günay, G.; Çörekçiöğlü, I. Konya-Karapınar Sinkholes (Obruks) of Turkey. In *Caves and Karst of Turkey—Volume 2: Geology, Hydrogeology and Karst*; Günay, G., Törk, K., Güner, İ.N., Gilli, E., Eds.; Springer International Publishing: Cham, Switzerland, 2022; pp. 27–39, ISBN 978-3-030-95361-4.
50. Bayari, C.S.; Pekkan, E.; Ozyurt, N.N. Obruks, as Giant Collapse Dolines Caused by Hypogenic Karstification in Central Anatolia, Turkey: Analysis of Likely Formation Processes. *Hydrogeol. J.* **2009**, *17*, 327–345. [[CrossRef](#)]
51. Orhan, O. Monitoring of Land Subsidence Due to Excessive Groundwater Extraction Using Small Baseline Subset Technique in Konya, Turkey. *Environ. Monit. Assess.* **2021**, *193*, 174. [[CrossRef](#)] [[PubMed](#)]
52. Kaya, B.; Aladağ, C. Precipitation, Temperature and Vegetation Relations in the Conditions of Konya. *J. Selçuk Univ. Soc. Sci. Inst.* **2009**, *22*, 265–278.
53. Sarıç, F.; Gedik, F. Meteorological Drought Analysis in Konya Closed Basin. *J. Geogr.* **2021**, *42*, 295–308. [[CrossRef](#)]
54. Demir, V.; Keskin, A.Ü. Height Modeling with Artificial Neural Networks (Samsun-Mert River Basin). *Gazi J. Eng. Sci.* **2020**, *6*, 54–61. [[CrossRef](#)]
55. Demir, V.; Keskin, A.Ü. Water Level Change of Lakes and Sinkholes in Central Turkey under Anthropogenic Effects. *Theor. Appl. Climatol.* **2020**, *142*, 929–943. [[CrossRef](#)]
56. Okay, A.I.; Tüysüz, O. Tethyan Sutures of Northern Turkey. *Geol. Soc. Lond. Spec. Publ.* **1999**, *156*, 475–515. [[CrossRef](#)]
57. Ulu, Ü. Geological Maps of Turkey Karaman-M30 Sheet. In *General Directorate of Mineral Research and Exploration*; General Directorate of Mineral Research and Exploration: Ankara, Turkey, 2009. (In Turkish)
58. Ulu, Ü. Geological Maps of Turkey Karaman-M31 Sheet. In *General Directorate of Mineral Research and Exploration*; General Directorate of Mineral Research and Exploration: Ankara, Turkey, 2009. (In Turkish)
59. Törk, K.; Erduran, B.; Yılmaz, N.P.; Sülükçü, S.; Güner, İ.N.; Ateş, Ş.; Mutlu, G.; Keleş, S.; Çınar, A.; Demirbaş, Ş.; et al. *Identification and Hazard Assessment of Karst Depression Areas in the Konya Basin*; Report No. 11250; MTA General Directorate, Geological Surveys Department: Ankara, Turkey, 2013.



60. Canik, B.; Arıgün, Z. Formation of Sinkholes around Karapınar-Kızören (Konya) and the Effect of Karapınar Volcanism on This Event. In Proceedings of the Karapınar Symposium, Karapınar, Turkey, 2001.
61. Erol, O. *Main Lines of Fourth Age (Quaternary) Geology and Geomorphology*; Faculty of Languages, History and Geography Publications: Ankara, Turkey, 1979.
62. Erol, O. The Relationships between the Phases of the Development of the Konya-Karapınar Obruks and the Pleistocene Tuz Golu and Konya Pluvial Lakes. In Proceedings of the Karst Water Resources Proceedings of the Ankara-Antalya Symposium, Ankara, Turkey, 7–19 July 1985; pp. 207–213.
63. Karabiyikoğlu, M.; Kuzucuoğlu, C.; Fontugne, M.; Kaiser, B.; Mouralis, D. Facies and Depositional Sequences of the Late Pleistocene Göçü Shoreline System, Konya Basin, Central Anatolia: Implications for Reconstructing Lake-Level Changes. *Quat. Sci. Rev.* **1999**, *18*, 593–609. [[CrossRef](#)]
64. Yıldırım, C. Relative Tectonic Activity Assessment of the Tuz Gölü Fault Zone; Central Anatolia, Turkey. *Tectonophysics* **2014**, *630*, 183–192. [[CrossRef](#)]
65. Esat, K.; Seyitoğlu, G.; Kaypak, B.; Koca-Çıvıgın, B.; Özdemirli, E.T. *What Do We Learn from the Recent Seismic Events about the Nature of Tuzgölü Fault Zone? Seismotectonics of the Tuzgölü Fault Zone under the Light of 2005–2007 Bala (M = 5.3; 5.4), 2020.07.12 (M = 3.5) Şereflikoçhisar and 2020.09.20 (M = 5.3) Obruk Earthquakes*; Researchgate Technical Report; Researchgate: Berlin, Germany, 2020.
66. Koçyiğit, A. The Denizli Graben-Horst System and the Eastern Limit of Western Anatolian Continental Extension: Basin Fill, Structure, Deformational Mode, Throw Amount and Episodic Evolutionary History, SW Turkey. *Geodin. Acta* **2005**, *18*, 167–208. [[CrossRef](#)]
67. Aksoy, R. Extensional Neotectonic Regime in West-Southwest Konya, Central Anatolia, Turkey. *Int. Geol. Rev.* **2019**, *61*, 1803–1821. [[CrossRef](#)]
68. Emre, Ö.; Duman, T.Y.; Özalp, S. *1:250,000 Scale Active Fault Map Series of Turkey, Karaman (N) 36-11*; Quadrangle: Ankara, Turkey, 2011.
69. Arık, F.; Bilgilioğlu, S.S.; İban, M.C.; Delikan, A.; Göçmez, G.; Döğen, A.; Kansun, G.; Gezgin, C.; Bilgilioğlu, H.; Dülger, A. *Sinkhole Technical Guide*; Tosun, Y., Çoruk, F., Arslan, Ş., Akkaya, Y., Gökçaya, E., Gökçaya, E., Eds.; Paradigm Academy Publications: London, UK, 2023; ISBN 978-625-6822-12-2.
70. Akbaş, B.; Akdeniz, N.; Aksay, A.; Altun, İ.E.; Balcı, V.; Bilginer, E.; Bilgiç, T.; Duru, M.; Ercan, T.; Gedik, İ.; et al. *1:1.250.000 Scaled Geological Map of Turkey*; General Directorate of Mineral Research and Exploration Publication: Ankara, Turkey, 2011.
71. Günay, G.; Güner, N.; Törk, K. Turkish Karst Aquifers. *Environ. Earth Sci.* **2015**, *74*, 217–226. [[CrossRef](#)]
72. Zanaga, D.; Van De Kerchove, R.; Daems, D.; De Keersmaecker, W.; Brockmann, C.; Kirches, G.; Wevers, J.; Cartus, O.; Santoro, M.; Fritz, S.; et al. *ESA WorldCover 10 m 2021 V200*; Zenodo: Honolulu, HI, USA, 2021.
73. Tapur, T. The Effects of the Old Konya Lake on the First Settlements. *Black Sea Stud.* **2009**, *6*, 99–115.
74. Lazecký, M.; Spaans, K.; González, P.J.; Maghsoudi, Y.; Morishita, Y.; Albino, F.; Elliott, J.; Greenall, N.; Hatton, E.; Hooper, A.; et al. LiCSAR: An Automatic InSAR Tool for Measuring and Monitoring Tectonic and Volcanic Activity. *Remote Sens.* **2020**, *12*, 2430. [[CrossRef](#)]
75. Morishita, Y.; Lazecky, M.; Wright, T.; Weiss, J.; Elliott, J.; Hooper, A. LiCSBAS: An Open-Source InSAR Time Series Analysis Package Integrated with the LiCSAR Automated Sentinel-1 InSAR Processor. *Remote Sens.* **2020**, *12*, 424. [[CrossRef](#)]
76. Yu, C.; Li, Z.; Penna, N.T.; Crippa, P. Generic Atmospheric Correction Model for Interferometric Synthetic Aperture Radar Observations. *J. Geophys. Res. Solid Earth* **2018**, *123*, 9202–9222. [[CrossRef](#)]
77. Şireci, N.; Aslan, G.; Çakır, Z. Long-Term Spatiotemporal Evolution of Land Subsidence in Konya Metropolitan Area (Turkey) Based on Multisensor SAR Data. *Turk. J. Earth Sci.* **2021**, *30*, 681–697. [[CrossRef](#)]
78. Gezgin, C. The Influence of Groundwater Levels on Land Subsidence in Karaman (Turkey) Using the PS-InSAR Technique. *Adv. Sp. Res.* **2022**, *70*, 3568–3581. [[CrossRef](#)]
79. Caló, F.; Notti, D.; Galve, J.P.; Abdikan, S.; Görüm, T.; Pepe, A.; Şanlı, F.B. DInSAR-Based Detection of Land Subsidence and Correlation with Groundwater Depletion in Konya Plain, Turkey. *Remote Sens.* **2017**, *9*, 83. [[CrossRef](#)]
80. Jones, C.E.; Blom, R.G. Bayou Corne, Louisiana, Sinkhole: Precursory Deformation Measured by Radar Interferometry. *Geology* **2014**, *42*, 111–114. [[CrossRef](#)]
81. John Upton Massive Louisiana Sinkhole Just Keeps on Growing. Available online: <https://grist.org/climate-energy/massive-louisiana-sinkhole-caused-by-oil-industry-just-keeps-on-growing/> (accessed on 7 December 2023).
82. Vassileva, M.; Al-Halbouni, D.; Motagh, M.; Walter, T.R.; Dahm, T.; Wetzell, H.-U. A Decade-Long Silent Ground Subsidence Hazard Culminating in a Metropolitan Disaster in Maceió, Brazil. *Sci. Rep.* **2021**, *11*, 7704. [[CrossRef](#)] [[PubMed](#)]
83. Jousset, P.; Rohmer, J. Evidence for Remotely Triggered Microearthquakes during Salt Cavern Collapse. *Geophys. J. Int.* **2012**, *191*, 207–223. [[CrossRef](#)]
84. Holzer, T.L. Ground Failure Induced by Ground-Water Withdrawal from Unconsolidated Sediment. *Rev. Eng. Geol.* **1984**, *6*, 67–105.
85. Garg, S.; Motagh, M.; Indu, J.; Karanam, V. Tracking Hidden Crisis in India's Capital from Space: Implications of Unsustainable Groundwater Use. *Sci. Rep.* **2022**, *12*, 651. [[CrossRef](#)]
86. Arık, F.; Dülger, A. *Sinkhole Basic Guide*; Paradigm Academy Publications: Çanakkale, Turkey, 2023.

- 
87. Schumann, H.H.; Cripe, L.S. Land Subsidence and Earth Fissures Caused by Groundwater Depletion in Southern Arizona, U.S.A. In Proceedings of the 3rd International Symposium on Land Subsidence, Venice, Italy, 19–25 March 1984; Johnson, A.I., Carbognin, L., Ubertini, L., Eds.; International Association of Hydrological Sciences Publisher: Wallingford, UK, 1986; Volume 151, pp. 841–851.
  88. Tihansky, A.B. Sinkholes, West-Central Florida. *US Geol. Surv. Circ.* **1999**, *1182*, 121–140.

**Disclaimer/Publisher’s Note:** The statements, opinions and data contained in all publications are solely those of the individual author(s) and contributor(s) and not of MDPI and/or the editor(s). MDPI and/or the editor(s) disclaim responsibility for any injury to people or property resulting from any ideas, methods, instructions or products referred to in the content.